# Revision 1 "An assessment of the reliability of melt inclusions as recorders of the pre-eruptive volatile content of magmas"

ROSARIO ESPOSITO[1,2]*, JERRY HUNTER[3], JAMES D. SCHIFFBAUER[4], NOBUMICHI SHIMIZU[5] AND ROBERT J. BODNAR[2]

[1]Dipartimento di Scienze della Terra, dell'Ambiente e delle Risorse, Università di Napoli Federico II, Napoli 80138, Italy

[2]Virginia Tech, Department of Geosciences, Blacksburg, Virginia 24061, USA

[3]Nanoscale Characterization and Fabrication Laboratory, Virginia Tech, Blacksburg, Virginia 24061, USA

[4]University of Missouri, Department of Geological Sciences, Columbia, Missouri 65211 USA

[5]Woods Hole Oceanographic Institution, Woods Hole, Massachusetts 02543-1050, USA

*Corresponding author: rosario.esposito3@unina.it

## ABSTRACT

Many studies have used melt inclusions (MI) to track the pre-eruptive volatile history of magmas. Often, the volatile contents of the MI show wide variability, even for MI hosted in the same phenocryst. This variability is usually interpreted to represent trapping of a volatile-saturated melt over some range of pressures (depths) and these data are in turn used to define a magma degassing path. In this study, groups of MI that were all trapped at the same time (referred to as a Melt Inclusion Assemblage, or MIA) based on petrographic evidence, were analyzed to test the consistency of the volatile contents of MI that were all trapped simultaneously from the same melt.

MIA hosted in phenocrysts from White Island (WI) (New Zealand) and from the Solchiaro eruption in the Island of Procida (Italy) were analyzed by Secondary Ion Mass Spectrometry (SIMS). In most MIA, $H_2O$, F and Cl abundances for all MI within the MIA are consistent (relative standard errors <27%, with the exception of two MIA), indicating that the MI all trapped a melt with the same $H_2O$, F, and Cl concentrations and that the composition was maintained during storage in the magma as well as during and following eruption. In several MIA, S abundances are consistent (relative standard errors <33%, with the exception of five out of 29 MIA). Conversely, $CO_2$ (WI and Solchiaro MIA) showed wide variability in several MIA. The result is that some MIA display a wide range in $CO_2$ content at approximately constant $H_2O$. Similar trends have previously been interpreted to represent degassing paths, produced as volatile-saturated melts are trapped over some significant pressure (depth) range in an ascending (or convecting) magma body. However, the $CO_2$ vs $H_2O$ trends obtained in this study cannot represent degassing paths because the MI were all trapped at the same time (same MIA). This requires that all of the MI within the MIA trapped a melt of the same composition (including volatile content) and at the same temperature and pressure (depth). The cause of the variable concentration of $CO_2$ within some MIA is unknown, but may reflect micrometer-scale heterogeneities within the melt during trapping, heterogeneities within individual MI, post-entrapment crystallization within the MI, formation of a shrinkage bubble associated with leakage/depressurization driven by cracks, or C-contamination during sample preparation. These results suggest that trends showing variable $CO_2$ and relatively uniform $H_2O$ obtained from MI may not represent trapping of volatile-saturated

melts over a range of pressure, and care must be taken when interpreting volatile contents of MI to infer magma degassing paths.

Results of this study have been used to estimate the uncertainties in volatile concentrations of MI determined by SIMS analysis. The $H_2O$, F, and Cl contents have an average estimated uncertainty of 11%, 9%, and 12 % respectively that is consistent with the SIMS analytical error. In contrast, the S and $CO_2$ contents have an average estimated uncertainty of 24% and 69% respectively that is not consistent with the SIMS analytical error.

Keywords:
melt inclusions
Melt Inclusion Assemblage (MIA)
pre-eruptive volatile contents
magma degassing path
Secondary Ion Mass Spectrometry

## INTRODUCTION

During the last several decades the number of publications describing the use of melt inclusions (MI) to determine the pre-eruptive volatile contents of magmas has increased significantly (Anderson et al., 1989; Audétat and Lowenstern, 2014; De Vivo and Bodnar, 2003; Lowenstern, 1995; Métrich and Wallace, 2008). In fact, MI provide the only direct method of determining the pre-eruptive volatile content of a magma. In many MI studies, the volatile contents of MI from the same sample (and sometimes from the same phenocryst) vary widely (Métrich and Wallace, 2008 and references therein).

Some workers have interpreted the variability in volatile concentration recorded by MI to be the result of crystals growing under varying pressure (depth) conditions in a volatile-saturated magma body that is ascending through the uppermost mantle or crust (Métrich and Wallace, 2008 and references therein).

Among all the volatile species, $CO_2$ contents generally show more variability compared to other volatiles (e.g., $H_2O$, Cl, F, S) and these results have been commonly interpreted as representing degassing of a $CO_2$-rich magmatic vapor from an ascending and crystallizing magma. This interpretation was first offered by Anderson et al. (1989), and has subsequently been invoked in numerous studies of MI. An extensive review of magma degassing systematics based on MI has been presented by Métrich and Wallace (2008). The model presented by Anderson et al. (1989) n requires that the crystallizing magma was volatile-saturated; thus, MI entrapped at greater depth are enriched in $CO_2$ while MI trapped at shallower depths are relatively depleted in $CO_2$, owing to the strong pressure effect on the solubility of $CO_2$ in silicate melt. Importantly, MI have been reported that not only show large variations in the $CO_2$ concentration in the same sample, but also in the same phenocryst (Anderson et al., 2000; Esposito et al., 2011; Hauri, 2002; Helo et al., 2011; Wallace et al., 1999). For instance, Helo et al. (2011) reported $CO_2$ contents of MI that range from 9,159 to 533 ppm (a range of 8,626 ppm) in MI hosted within the *same* plagioclase crystal – this requires that the plagioclase crystal grew (and trapped MI) over a pressure range of ~1,000 to <100 MPa, or a depth range of ~30-35 km to ~3-4 km.

.

Similarly, Anderson et al. (2000) reported $CO_2$ contents ranging from 209 to 761 ppm for MI within a single quartz phenocryst from the Bishop Tuff, with the higher $CO_2$ concentrations in MI near the phenocryst rim, i.e., the latest MI trapped (see their Fig. 3). Based on the paragenesis consisting of MI with higher $CO_2$ contents trapped later in the growth history, Anderson et al. (2000) interpreted the $CO_2$ variation to be the result of crystal growth as the phenocrysts were sinking in the magma and trapping MI from a volatile-saturated melt Peppard et al. (2001). Anderson et al. (2000) thus argued that the inverted $CO_2$ vs $H_2O$ trend is due to crystal settling during phenocryst growth in a large, convecting magma chamber, rather than the result of magma ascending through the crust. Roberge et al. (2013) observed reversed trends in the variation in $CO_2$ contents of MI from the Bishop tuff similar to those observed by Anderson et al. (2000). In contrast to Anderson et al. (2000), Roberge et al. (2013) interpreted the trends to indicate that a later, $CO_2$-rich (deep) magma invaded the shallower, $CO_2$-poor magma reservoir. This suggests that less evolved deep magmas recharging shallow reservoirs may contribute to the range in $CO_2$ concentrations recorded by MI trapped within a single phenocryst. However, the variations in $CO_2$ content should correlate with variations in major and trace element chemistry that are consistent with mixing of a less evolved magma with one that is more evolved.

The use of MI to infer the volatile history of a magma is based on the assumption that MI trap a representative sample of the melt from which the phenocryst was growing, and that the MI preserve the composition after entrapment, and several studies have attempted to test these assumptions (Métrich and Wallace, 2008 and references therein). For example, the composition of the melt trapped in MI depends on the interplay of

diffusion of cations away from or towards the melt/crystal interface, and on crystal growth rates (boundary layer effect). Some workers have documented that MI are affected by boundary layer processes under some conditions and do not trap a representative sample of the bulk melt. This assertion is based on the assumption that MI are generally trapped during periods of rapid growth caused by abrupt changes in temperature, pressure and volatile exsolution rate, as might occur during an eruptive event (Roedder, 1979). The effect of growth rate on MI characteristics was studied by Faure and Schiano (2005), who synthesizedolivine at different growth rates. These workers found that MI hosted in polyhedral olivine recorded consistent major element compositions, regardless of their size. Conversely, olivine showing skeletal and dendritic morphology (produced by the most rapid growth rates) contained MI that were enriched in $Al_2O_3$, suggesting that the growth rate was sufficiently fast that Al could not diffuse away from the growing crystal surface to maintain equilibrium with the bulk melt. However, other studies show no enrichment of $Al_2O_3$ in MI, relative to the bulk rock (Spilliaert et al., 2006; Vigouroux et al., 2008). Additionally, Luhr (2001) reported that MI hosted in olivine that grew rapidly do not show $Al_2O_3$ enrichment similar to that reported by Faure and Schiano (2005). Conversely, Baker (2008) showed that elements that diffuse slowly (e.g., $P_2O_5$) can be enriched in a boundary layer melt that is trapped as MI. Baker suggested that a good test of whether boundary layer processes were affecting the MI composition was to examine the concentration ratios of slow diffusing elements to fast diffusing elements (e.g., $P_2O_5$/Cl). Kent (2008) and Esposito et al. (2011) found no correlation between concentrations of large cations (K, Ba, Pb) and MI size, indicating that boundary layer effects have influenced the MI compositions. Similarly, Wardell et al.

(2001) found no correlation between volatile concentrations and MI size, suggesting that boundary layer processes did not affect volatile concentrations of MI from White Island. Some workers note that MI could be trapped during dissolution-reaction-mixing when a basaltic magma interacts with a colder plagioclase-bearing mush zone (Danyushevsky et al., 2004; Esposito et al., 2011). These MI, which usually represent only a small fraction of the total MI population, show anomalous compositions and are usually ignored during reconstruction of magma chemistry.

Several studies have focused on processes that may have modified MI after trapping (Danyushevsky et al., 2002; Gaetani et al., 2012; Roedder, 1979; Severs et al., 2007; Steele-MacInnis et al., 2011). For example, it is well known that some crystallization may (must?) occur at the MI/host interface if the temperature decreases after the MI is trapped and before it is naturally ejected and quenched. This phenomenon is known in the literature as post-entrapment crystallization (PEC). Steele-MacInnis et al. (2011) developed a thermodynamic model to predict the evolution of $CO_2$ and $H_2O$ contents of the melt (glass) as a result of PEC. These workers demonstrated that, with relatively small amounts of PEC (<10%), most of the $CO_2$ originally dissolved in the trapped melt would exsolve from the melt during PEC and reside in the vapor bubble. In agreement with the results of Steele-MacInnis et al. (2011), Esposito et al. (2011) found that 64% of the $CO_2$ in the original melt that was trapped as an inclsusion was contained in the vapor bubble of a MI from the Solchiaro eruption on the Island of Procida, Italy. Other researchers have reported that the $CO_2$ contents of glasses in bubble-bearing MI likely provide a minimum estimate of the original $CO_2$ content of the melt trapped in the MI. For instance, Kamenetsky et al. (2007) detected C in MI in the form of a $CO_2$

159 gaseous phase as well as a carbonate phase. Anderson and Brown (1993) reported that
160 inclusions 100 μm in diameter trapped in olivine from the 1959 Kilauea Iki eruption
161 contain $CO_2$ gas and liquid with a bulk density of at least 0.3 g/cm$^3$. Anderson and Brown
162 (1993) corrected the trapping pressure of the MI by adding back into the melt (glass)
163 phase the $CO_2$ amount that would be contained in a bubble occupying 0.5 volume % of
164 the MI at the trapping conditions. Finally, Moore et al. (2013) detected $CO_2$ in the vapor
165 bubble in most of the MI from Kilauea Iki that they analyzed, and estimated that ~10 to
166 >90% of all of the $CO_2$ in the MI is contained in the vapor bubble.

167 While it is sometimes possible to correct for the effect of PEC on volatile contents
168 of MI, for some host phases these corrections are complicated by post-entrapment
169 diffusion of elements into or out of MI (Danyushevsky et al., 2002; Gaetani et al., 2012).
170 For instance, Gaetani et al. (2012) have shown that H can diffuse out of the MI and
171 through the olivine host in a relatively short time if there is a $P_{H2O}$ gradient with the
172 surrounding melt ($H_2O$-degassed melt). Thus, depending on where MI occur relative to
173 the core and rim of the host, the volatile contents of MI in the same phenocryst may be
174 affected to different extents. This, in turn, could lead to widely variable volatile contents
175 in MI that originally all had the same concentrations.

176 Several models have been developed to correct the compositions of MI that show
177 disequilibrium with the host (Danyushevsky et al., 2002; Gaetani and Watson, 2002;
178 Kress and Ghiorso, 2004). These models can be applied to correct MI major element
179 compositions of well-studied silicate melt/crystal systems (e.g., olivine/silicate melts). It
180 is important to note that both (1) modification of volatile contents of MI due to diffusion
181 and (2) modification of volatile concentrations due to PEC and formation of a vapor

bubble can produce $H_2O$-$CO_2$ trends similar to those produced by trapping of MI during ascent-driven magma degassing.

Based on the many factors described above that may alter the original volatile contents of MI, it is important to test the reliability of volatile contents obtained by analysis of MI. In fluid inclusion (FI) research, a well-defined and tested protocol has been developed that allows researchers to be confident that the data obtained from FI record the physical and chemical conditions of the fluid at the time of trapping. As such, a group of FI that were all trapped at the same time (i.e., all trapped a fluid of the same composition, and at the same PT conditions) is defined as a Fluid Inclusion Assemblage, or FIA (Bodnar, 2003; Goldstein and Reynolds, 1994). If the FI all trapped a single homogeneous phase and have not reequilibrated (compositionally or volumetrically) following entrapment, all inclusions in the FIA should show identical compositions and microthermometric behavior when studied in the lab. For FI, evidence of contemporaneous trapping is provided when several inclusions occur along a crystal growth surface or along a healed fracture. Bodnar and Student (2006) described a similar methodology to study MI, and proposed the term *Melt Inclusion Assemblage* (MIA) to define a group of MI that were all trapped at the same time. In practical terms, an MIA is represented by a group of MI that occur along the same growth zone in a phenocryst, or in a three-dimensional cluster within the crystal, because MI are less commonly trapped along healed fractures, compared to fluid inclusions. The accepted methodology in FI studies is to only collect data from FIAs. In contrast, MIA are rarely studied in MI studies because MIA are generally less common than FIAs, with many phenocrysts containing only one or perhaps a few MI. Moreover, the methods used to study MI (especially the

volatile contents) require that the MI be exposed on one surface (SIMS and Raman) or on two surfaces (FTIR), and it is challenging to simultaneously expose more than one MI from the same crystal. Finally, because analysis by FTIR requires that the MI be exposed on both surfaces of the host phenocryst (however, see Lowenstern and Pitcher, 2013), most of the phenocryst (and its contained MI) is destroyed during polishing to expose the MI on both the top and bottom surfaces, and this reduces the likelihood that more than one MI in each crystal will be available for analysis.

In this study, we present results of volatile ($CO_2$, $H_2O$, F, S, and Cl) analyses of MI from several different MIA to test the fidelity of the MI technique for recording the volatile history of an evolving magma. The examined MIA are hosted in phenocrysts from the active White Island volcano in New Zealand and from the Solchiaro volcano on the Island of Procida (southern Italy). Major and trace element contents of MI from White Island samples have been reported by Rapien et al. (2003), Severs et al. (2009) and Wardell et al. (2001), while major/trace element and volatile contents of MI from Solchiaro were presented by Esposito et al. (2011) and Mormone et al. (2011). Importantly, Rapien et al. (2003) and Severs et al. (2009) reported that major and trace element compositions of MI within MIA from White Island do not show significant variations, suggesting that the MI all trapped the same melt and have not reequilibrated following entrapment.

## GEOLOGICAL BACKGROUND

Samples analyzed in this study are from two recent eruptions (1986 and 1988; Rapien et al., 2003) at White Island, New Zealand and from the Solchiaro eruption on Procida

Island, Italy that occurred between 19.6 and 14.3 Ka (Alessio et al., 1989; Lirer et al., 1991). Below we summarize the petrological and geochemical data for the samples considered in this study.

**White Island, New Zealand**

White Island is an active volcano located on the active margin between the Australian plate and the Pacific plate (Isacks et al., 1968). White Island is located at the northern end of the Taupo Volcanic Zone (TVZ) in the Bay of Plenty, and has been active since Late Pleistocene (Graham et al., 1995). Two of the more recent eruptive cycles are the 1976–1982 and 1986–1992 events during which the eruptive style alternated between phreatomagmatic and strombolian. On July 27$^{th}$, 2000 the most recent eruption blanketed the island with scoriae. The 1976–1982 and 1986–1992 activity has been associated with a large magma body (approximately $10^6$ $m^3$) that ponded at around 0.5 km depth (Clark and Cole, 1989). The samples studied here are ejected scoriae and were collected by Dr. C. Peter Wood of the Institute of Geological and Nuclear Sciences, Wairakei, New Zealand. These same White Island samples have been described in detail by Rapien et al. (2003), Rapien (1998), and Severs et al. (2009).

Volcanic products at White Island range from mafic andesite to dacite and activity can be divided into 5 cycles (Cole et al., 2000). Each cycle starts with more mafic compositions and ends with dacitic products. Lavas erupted at White Island are medium-K, calc-alkaline in composition (Cole et al., 2000; Graham and Cole, 1991; Graham et al., 1995). Whole rock analyses reported by Graham et al. (1995), Cole et al. (2000) and Graham and Cole (1991) are from the 1977 eruption and, to our knowledge, no whole-rock data are available for the later erupted material (younger than 1977). The studied

samples are vescicular porphyritic andesite-dacite and contain plagioclase, clinopyroxene and orthopyroxene as the major phenocryst phases from 50 to 70 volume percent of the rock (Rapien, 1998; Rapien et al., 2003; Severs et al., 2009). Compositions of representative phenocrysts from the 1977, 1986, 1988, and 1991 eruptions have been reported by several researchers (Graham and Cole, 1991; Rapien, 1998; Rapien et al., 2003; Severs et al., 2009; Wardell et al., 2001). Rapien (1998) and Rapien et al. (2003) reported that the anorthite content of plagioclase phenocrysts ranges from $An_{68}$ and $An_{62}$, while plagioclase inclusions in orthopyroxene and clinopyroxene show a wider range of anorthite content, from $An_{74}$ to $An_{62}$ (1977, 1888, 1989, 1991 WI eruptions). Severs et al. (2009) reported an average anorthite composition of $An_{67}Ab_{31}Or_2$ for the 1988 WI eruption. Wardell et al. (2001) reported similar plagioclase compositions ($An_{63}Ab_{35}Or_2$). Rapien (1998) and Rapien et al. (2003) reported pyroxene compositions of $En_{69\text{-}72}Fs_{23\text{-}26}Wo_{3\text{-}5}$ for orthopyroxene, and $En_{45\text{-}46}Fs_{14\text{-}16}Wo_{38\text{-}40}$ for clinopyroxene. Wardell et al. (2001) reported similar orthopyroxene ($En_{70}Fs_{26}Wo_4$) and clinopyroxene ($En_{46}Fs_{16}Wo_{38}$) compositions for the 1989 eruption. Severs et al. (2009) reported average compositions of $En_{71}Fs_{27}Wo_2$ for orthopyroxene, and $En_{47}Fs_{13}Wo_{40}$ for clinopyroxene. Graham and Cole (1991) studied mafic-andesite blocks and bombs erupted in 1977 and reported more primitive compositions of $En_{68\text{-}78}Fs_{18\text{-}28}Wo_4$ for orthopyroxene, and $En_{47\text{-}51}Fs_{10\text{-}15}Wo_{38\text{-}39}$ for clinopyroxene, with anorthite contents of plagioclase up to $An_{75}$. Plagioclase and pyroxenes show slight reverse zoning, and some plagioclase phenocrysts from the 1989 eruption show cores with patchy zonation (Wardell et al., 2001). Rapien (1998) and Rapien et al. (2003) found no zoning in phenocrysts from the 1977, 1986, 1988, 1989, and 1991 eruptions when observed using back-scatter electron imaging, but chemical

zonation in plagioclase was revealed by differential interference contrast microscopy after etching in fluoboric acid (Figure 3 in Rapien, 1998). Rapien (1998) noted that MI and mineral inclusions are trapped along bands defined by fluoboric acid etching. MI in the same growth zone within a single phenocryst show a narrow range in major element concentrations (Figure 12 in Rapien, 1998), trapped along growth zones represent an MIA, i.e., were all trapped at the same time, and from the same melt. Using the software MELTS (Asimow and Ghiorso, 1998; Ghiorso and Sack, 1995), Severs et al. (2009) calculated that the dacitic melts produced at White Island resulted from 50% fractional crystallization of the less evolved andesite at White Island. The compositions of clinopyroxene and orthopyroxene predicted by MELTS are consistent with that of White Island dacitic samples, but the predicted plagioclase composition is slightly less anorthitic than that found in White Island dacitic samples ($An_{60}$ vs. $An_{67}$).

Several studies have reported the occurrence of MI along growth zones in phenocrysts from recent eruptions of White Island (Cole et al., 2000; Rapien, 1998; Rapien et al., 2003; Severs et al., 2009; Wardell et al., 2001). And, MI occurring along growth zones in plagioclase and in pyroxenes show consistent major and trace element concentrations (Fig. 1). The uniformity in major and trace element contents of MI in a given growth zone, i.e., MI that were all trapped at the same time, provides strong evidence that the MI composition represents the composition of the melt that the phenocryst was precipitating from, without modification from boundary layer processes or later post-entrapment modifications. In light of the fidelity of MI in recording the composition of the bulk melt that was precipitating the phenocrysts, (Severs et al., 2009) calculated partition coefficients between dacitic melt and plagioclase and between dacitic

melt and pyroxene based on data from 87 MI from the 1988 eruption, and found no significant variation in major and trace elements composition as a function of host mineral. For instance, MI hosted in clinopyroxene phenocrysts show the same CaO concentration as MI hosted in orthopyroxene (Fig. 1f), suggesting that boundary layer processes did not affect MI compositions. If boundary layer processes had affected the MI compositions, one would expect the CaO content of MI in clinopyroxene to be depleted relative to that of MI in orthopyroxene because Ca is compatible in clinopyroxene but incompatible in orthopyroxene. The same logic applies to MgO or $FeO_{tot}$ contents of MI hosted in plagioclase vs. MgO or $FeO_{tot}$ of MI hosted in clino/orthopyroxene; the average concentrations of MI in all three phases are the same, within analytical error (Fig. 1b, d, f). If boundary layer processes significantly affected the MI compositions, one should expect FeO and MgO concentrations of MI hosted in plagioclase to be enriched relative to concentrations of MI hosted in the pyroxenes. We note that Wardell et al. (2001) reported that variations in major element abundances of MI versus $SiO_2$ content are consistent with fractional crystallization. Wardell et al. (2001) did, however, report more variability in composition, relative to compositions reported by Rapien (1998) and Severs et al. (2009). MI from White Island show FeO concentrations that are consistent with geochemical trends defined by bulk rocks from White Island (Fig. 1a and b), suggesting that post-entrapment Fe-loss or gain did not occur. It is important to note that all MI from White Island that were analyzed show low $H_2O$ (< 1 wt%) and low S concentrations (often ≤ 200 ppm) (Rapien, 1998; Wardell et al., 2001).

**Solchiaro eruption, Procida Island, Italy**

Solchiaro is an inactive volcano  well-documented volcanic history (Cecchetti, 2001; D'Antonio et al., 1999; De Astis et al., 2004; Di Girolamo et al., 1984; Esposito et al., 2011; Mormone et al., 2011). The Solchiaro vulcanites are part of the potassic rock series that outcrops in the Island of Procida (Phlegrean Volcanic District, Campanian magmatic province). De Astis et al. (2004) subdivided the Solchiaro deposits into three units, and the eruptive style changed during the eruption from phreatomagmatic (represented by unit I deposits) to increasingly strombolian products in units II and III. The composition of Solchiaro products varies from trachybasalt (unit I) to shoshonite (unit II and III). Esposito et al. (2011) studied the geochemical evolution of products associated with unit I of the Solchiaro eruption, based on MI data. In contrast to MI from the recent eruptions at White Island, MI from Solchiaro show a wide range in major and trace element concentrations, even within a single crystal (Esposito et al., 2011; Mormone et al., 2011). Also, the forsterite content of olivine shows a wide variation, from $Fo_{81}$ to $Fo_{90}$ (Esposito et al., 2011) or from $Fo_{85}$ to $Fo_{90}$ (Mormone et al., 2011), and some olivines show chemical zoning. Esposito et al. (2011) also found anomalous MI that they referred to as "Sr-rich" MI and "Enriched" MI. The anomalous MI were interpreted to have been trapped during olivine growth in a plagioclase-bearing mush zone where dissolution reaction - mixing occurred. It is important to note that only 12 out of 109 MI studied had anomalous compositions. Some MI also show post-entrapment modifications, including Fe-loss due to diffusion and PEC, as evidenced by a negative trend in Fo mole% vs. $FeO_{tot}$ (Fig.3a in Esposito et al., 2011). On the other hand, Mormone et al. (2011) reported some MI showing $FeO_{tot}$ concentrations much higher than concentrations

obtained from whole rock analysis. Volatile concentrations of MI show significant variation, especially for $CO_2$, and it has been interpreted to be the result of olivine crystallization from an ascending $H_2O$-$CO_2$ saturated magma (Esposito et al., 2011; Mormone et al., 2011). Esposito et al. (2011) reported that bubble-free MI in one sample (RESC5) show a good correlation for $CO_2$ vs. crystallization indicators (Fig. 2), consistent with this interpretation. In addition, Esposito et al. (2011) have analyzed two MI trapped along a growth zone and, thus, within the same MIA. These two MI (RESC5-O21-MA and ME) show the same major and trace elements and volatile composition considering the analytical errors (Table 1 and Fig. 2b).

The two samples used in the present study (RESC2 and RESC5) are gray tuffs from Solchiaro unit I that have been described by Esposito et al. (2011).

## SAMPLE PREPARATION AND ANALYTICAL METHODS

Most of the phenocrysts from White Island and Solchiaro were prepared as described by Esposito et al. (2011).

Only MIA in which the MI were > 20 μm in diameter were selected, owing to the minimum spot size required for Secondary Ion Mass Spectroscopy (SIMS) analyses.

After an MIA was identified petrographically, the crystal containing the MIA was mounted on a glass bar or in a one-inch epoxy mount to expose as many of the MI within the MIA as possible. After one (or more) MI was exposed, the phenocryst was removed from the glass rod/epoxy and mounted in a round, one-inch diameter indium microprobe mount. Indium was used to mount the crystals for SIMS analysis because, at the high vacuum of the SIMS, epoxy can outgas and contaminate the sample with H, C and O.

Following analysis of the exposed MI(s), if the MIA contained additional MI that were deeper in the sample, i.e., not exposed at the surface, the crystal hosting the MIA was removed from the indium mount and polished again to expose additional MI in the same MIA. The same crystal was then remounted in indium and the newly exposed MI were analyzed. This process was repeated until all suitable MI (i.e., glassy MI >20 μm) within the MIA had been analyzed.

Before SIMS analysis, all exposed MI were examined with the SEM as described in Esposito et al. (2011) to test for chemical homogeneity. For SEM analysis, a gold coating was used, rather than a carbon coating, to avoid possible carbon contamination that could lead to incorrect values for $CO_2$ during SIMS analysis. We did not analyze major or trace elements in the MI because other workers have extensively studied the major and trace element chemistry of these samples, as summarized above (Esposito et al., 2011; Rapien et al., 2003; Severs et al., 2009). Before analysis of MI in plagioclase by SIMS, the sample was placed into the sample cell of a laser ablation - inductively coupled - plasma mass spectrometer (LA-ICP-MS) and the laser was used to ablate (drill) small holes around each MI (Fig.3). These holes were placed strategically around the MI and a photograph was made of each MI and its "locator holes" – this was necessary to locate the MI during SIMS analysis because the glass and host plagioclase are similar in reflected light. In the absence of the ablation pits, it was often not possible to locate MI hosted in plagioclase using the viewing optics on the SIMS.

Volatile concentrations ($CO_2$, $H_2O$, F, S, and Cl) of MI were obtained in two different SIMS facilities, using the IMS 7f-GEO at Virginia Tech and the Cameca IMS 1280 at the Woods Hole Oceanographic Institution (WHOI). Data were collected during eight

working sessions: May 2008, December 2008, March 2010, December 2010, February 2011, October 2011, March 2012, and January 2013. The Cameca IMS 1280 at WHOI was used only for the February 2011 and January 2013 working sessions. We note that one of the anonymous reviewers of an earlier version of this manuscript raised concerns about our use of two different SIMS laboratories in this study, suggesting that we would have observed less variation if the same laboratory and instrument had been used for all analyses. While our results may have been more precise had we used a single laboratory, in this study we are interested not only in the precision of the measurements but also in the accuracy. Thus, if both laboratories are producing results of comparable accuracy, it should not matter if two labs are used. And, by using two separate laboratories, we are able to determine with reasonable certainty that the variations observed are not instrument (or laboratory) specific or artifacts but of the sample preparation and analysis methods are, in fact, real.

During earlier working sessions (May 2008, December 2008, March 2010), acetone was used during sample preparation. During later working sessions (December 2010, February 2011, October 2011, March 2012, and January 2013), acetone was not used to avoid potential C deposition in microfractures, especially at the MI/host interface. It is important to note that $CO_2$ variability within a single MI does not correlate with working session, i.e., is independent of whether acetone was or was not used during sample preparation.

Before SIMS analysis at Virginia Tech, the indium mounts were cleaned in deionized water in an ultrasonic bath and were dried in a vacuum-oven for 12 hours. Each sample was gold-coated (sputter coating) and the thickness of the coating was ~300 Å for the

411 SIMS analysis. Working sessions at Virginia Tech used Cs as the primary ion source with
412 a beam current between 1 and 1.6 nA. Each analytical spot was pre-sputtered for 290 s to
413 clean the surface before analysis. The rastered area was 30 μm by 30 μm for each
414 analysis, and a 15 μm by 15 μm spot within the rastered area was analyzed 10 to 15 times
415 in depth profile mode. Masses $^{16}O^{1}H$, $^{12}C$, $^{19}F$, $^{32}S$, or $^{35}Cl$ and $^{30}Si$ were measured, and
416 concentrations were related to the ratio of each mass of interest to $^{30}Si$. Five standard
417 glasses were used to calibrate the instrument for $H_2O$, $CO_2$, F, S, and Cl (Appendix Table
418 1 Deposit Item-01). The standards represent natural basaltic and basaltic-andesitic
419 glasses. Additional information on the glass standards can be found in Helo et al. (2011).
420 In some cases, the standard glasses were measured multiple times. For instance, the
421 standard glass GL07-D52-5 ($CO_2$ = 88 ppm) was analyzed 10 different times (five times
422 before MI analysis and five times after MI analysis) and the relative 1 sigma error was
423 22% (Appendix Table 1).

424 To test for systematic variations in $CO_2$ distribution within MI, we performed depth
425 profiling in some of the MI during the March 2012 working session. During this working
426 session, the analytical settings were modified to optimize the depth resolution for the C
427 isotope. Specifically, the $^{12}C$ and $^{30}Si$ (used as reference) secondary ions were detected
428 using 15kV $^{133}Cs+$ primary ion bombardment at a 24º incident angle using 20 nA current.
429 To avoid undesired signal from the edge of the raster, the primary beam was rastered over
430 an area 75 μm by 75, μm and a detected area of 16 μm by 16 μm was used. A normal
431 incidence electron beam was used to compensate for positive charging of the sample
432 surface. A mass resolving power of 2000 m/dm was used to resolve possible interferences
433 with the $^{12}C$ signal. At the conditions used, we estimated a sputtering rate of ~1 μm per

1000 second, or 1nm per second. For the SIMS at Virginia Tech, the 1 sigma errors based on the slope of each calibration line are 12% relative for $CO_2$, 20% for $H_2O$, 12% for F, 9% for S, and 11% for Cl over a period of almost four years. During SIMS analysis, each MI was monitored using the time-resolved "ion response screen" to test for anomalous ion distribution. In some cases we noted heterogeneity in the distribution of C in the MI. These anomalous screen responses sometimes result in unrealistically high concentrations (e.g. up to 5 wt % of $CO_2$), and we observed that MI showing this behavior also often showed fractures that apparently were introduced during polishing. We further note that a heterogeneous distribution is sometimes observed when the probe spot is not well centered in the MI (analytical area close to the wall of the MI or including some of the surrounding host phase). Therefore, we excluded all analyses that showed heterogeneity in the ion-response during the SIMS analysis because we interpreted this behavior as being due to contamination and/or improper beam placement. This interpretation must be treated with caution because it is possible that the variable and elevated $CO_2$ concentration might be real and represent anomalous (and unexplained) concentrations of $CO_2$ in MI, as discussed below.

The analytical conditions used for the working sessions at WHOI (February 2011 and January 2013) were similar of those used at Virginia Tech, and are described in more detail by Helo et al. (2011). Four standard glasses were used during the February 2011 session, and three of these were analyzed multiple times (see Appendix Table 1 and Deposit Items-01). The standard glasses used for the calibrations are basalt and andesitic basalt composition; further details can be found in Helo et al. (2011). Based on four analyses on one of the standard glasses (GL07 D52-5), the 1-sigma reproducibility is 6%

for S and F, 14% for Cl, and 16% for $CO_2$ and $H_2O$. The standard glasses used at Virginia Tech are from the same set used at the WHOI. For the January 2013 working session, nine standard glasses were used and the calibration data are reported in Appendix Table 1 and Deposit Item-01. The more interesting feature of the calibration data for the January 2013 session is that a $CO_2$-rich standard glass (3154 ppm, NS1) and an $H_2O$-rich standard glass (2.49 wt%, JDH 17H) were included. The $CO_2$-rich and the $H_2O$-rich standard glass data are consistent with the calibration curves obtained in previous working sessions (Deposit Item-01). For the January 2013 session, a standard glass (ALV 519-4-1, see Appendix Table 1) was measured multiple times during the MI analysis. The 1-sigma errors of volatile concentrations measured on this glass standard are all < 5%.

During all working sessions, the concentrations of $CO_2$ measured in a quartz blank (mounted with standard glasses) and in plagioclase, clinopyroxene and olivine (adjacent to MI) were always lower than those measured in the MI glass (see Appendix Table 1). After SIMS analysis, all samples were examined under the optical microscope to confirm that the beam had been completely within the MI during the analysis. If the beam was not completely contained within the MI, the data were discarded. Note, however, that it was usually not possible to determine how close the bottom of the analytical pit was to the MI/host interface at depth.

Focused Ion Beam Electron Microscopy (FIB-EM) was used to study the morphology of a few MI in three dimensions. A beam current between 0.043 and 1.4 nA and voltage of 5 kv was used for imaging the MI. The sample was tilted 52° before the images were captured as described by Schiffbauer and Xiao (2009) and (2011).

# RESULTS

## Petrography

Phenocrysts (clinopyroxene, plagioclase, and orthopyroxene in increasing order of abundance) from the White Island samples were separated from vesicular porphyritic andesitic scoria. The phenocryst size ranges from 0.5 to 3 mm and the habit is predominantly euhedral (Fig. 4). SEM images of the phenocrysts show no evidence of chemical zoning with exception of one plagioclase phenocryst. Rapien et al. (2003) reported that etching in fluoboric acid reveals that, although zoning is not usually recognized during normal petrographic examination, plagioclase phenocrysts are zoned and that MI occur along zones defined by the etching. Wardell et al. (2001) reported that cores of some plagioclase phenocrysts from the 1989 scoriae show spongy textures when observed with backscattered electron imaging. In particular, MI hosted in the cores of plagioclase phenocrysts from the 1989 scoriae show less evolved major element compositions compared to MI at the rims of the same plagioclase phenocrysts (Wardell et al., 2001). In contrast, Rapien (1998) found no correlation between MI position within phenocrysts and MI composition in scoriae from the 1977, 1986, 1988, and 1989 White Island eruptions. In most phenocrysts, solid and melt inclusions coexist and are aligned along crystal growth faces (Fig. 3 and 4). Clinopyroxene phenocrysts contain plagioclase and orthopyroxene mineral inclusions, orthopyroxene phenocrysts contain clinopyroxene and plagioclase inclusions, and plagioclase phenocrysts contain clinopyroxene inclusions. We did not observe orthopyroxene inclusions in plagioclase, but Rapien et al. (2003) reported rare orthopyroxene inclusions in plagioclase. These occurrences suggest that the clinopyroxene, plagioclase and orthopyroxene were co-crystallizing and were likely in

503 equilibrium during crystallization of the White Island magma, as was also noted by
504 Rapien et al. (2003) and by Severs et al. (2009). Apatite inclusions are common in all
505 three phenocrysts. Magnetite was observed occasionally as inclusions in clinopyroxene,
506 as also reported by Rapien et al. (2003).

507 MI are ubiquitous in clinopyroxene, plagioclase and orthopyroxene phenocrysts. Four
508 main types of MI were recognized: (1) MI containing only glass are referred to here as
509 type 1 MI, (2) MI containing glass plus one or more trapped minerals are referred to here
510 as type 2 MI, (3) MI containing glass plus a vapor bubble or a vapor bubble plus one or
511 more trapped minerals are referred to here as type 3 MI, (4) MI containing a sulfide
512 globule (originally an immiscible sulfide melt?) or a sulfide globule plus a vapor bubble
513 are referred to here as type 4 MI. The mineral inclusions in type 2 MI are not considered
514 to be daughter crystals because the area (volume) ratios between the mineral and the glass
515 range from ~0.1 to 1, suggesting trapping of various proportions of melt and crystals.
516 Crystallized MI or partially crystallized MI were not observed in the samples studied.
517 The presence of bubbles in some MI (type 3) suggests that they were either trapped along
518 with the mineral and melt, or the bubbles nucleated due to PEC or as a result of cooling
519 during eruption. Sulfide-bearing MI (type 4) are observed in clinopyroxene and
520 orthopyroxene but not in plagioclase, and they are found only in the cores of these
521 phenocrysts.

522 Most of the MI shape includes negative-crystal shaped or ovoid to spherical shapes,
523 but some MI show irregular shape. In order to better characterize the 3-dimensional
524 geometry of MI, vertical sections were excavated through or adjacent to a few MI using
525 the Focused Ion Beam Electron Microscope (FIB-EM). The excavations range from ~5 to

526 ~15 μm in depth and MI shape was observed to vary from ovoid to prismatic (Fig. 5).
527 The MI geometry in three dimensions can only be approximated because only one cross-
528 section through each MI was available from the FIB-EM analysis.

529 In most cases, MI of all types occur along growth zones or in the cores of phenocrysts
530 (Fig. 3 and 4). MI entrapped along growth zones are referred to as *zonal* MI and are
531 interpreted by Sobolev and Kostyuk (1976) to be primary MI trapped during growth of
532 the phenocryst. MI clustered in the cores of phenocrysts are defined as *azonal* MI and are
533 also interpreted to be primary by the same workers. In two cases, we noted trails of MI
534 with elongated shape and assume that these were trapped when two phenocrysts of the
535 same mineral joined together during continued growth (pseudo-secondary MI, Deposit
536 Item-02).

537 In this study, groups of MI trapped along the same growth zone (zonal MI) or
538 clustered in the core (azonal MI) are interpreted to represent MIAs, that is, groups of MI
539 that were all trapped at approximately the same time (see Appendix Table 2). While MI
540 in both zonal and azonal occurrences are interpreted to have been trapped "at the same
541 time", the length of time required to trap azonal MIA may have been longer than that
542 required for zonal MIA formation. In the White Island phenocrysts, some MIA are
543 composed only of type 1 MI (MI containing only glass), other MIA are composed only of
544 type 2 MI (MI containing glass plus one or more crystals), and some other MIA can
545 contain all types of MI (Appendix Table 2). It is important to note that the different types
546 of zonal MIA can alternate in the same phenocryst as is commonly observed in
547 plagioclase (Fig. 3). Azonal MIA often include more than one type of MI, while zonal
548 MIA are mostly represented by only one type of MI (type 1 or type 2 MI). Classifications

549 of individual (types 1, 2, 3 or 4, and shapes) and MIA (zonal or azonal) studied are listed
550 in Appendix Table 2.

551 MI from the Solchiaro samples contain naturally quenched glass and were previously
552 described by Esposito et al. (2011). Five of the phenocrysts previously analyzed by
553 Esposito et al. (2011) were selected for analysis of additional MI in the same MIAs. The
554 MI shape is variable and includes irregular, negative-crystal shaped and sometimes ovoid
555 to spherical shapes. FIB-SEM examination of one MI hosted in olivine shows an irregular
556 MI/host interface (Fig. 6). In most cases, MIA are defined by MI that range from 3 to 10
557 μm and are thus too small to be analyzed with the SIMS. However, we did identify six
558 MIA containing MI that were large enough for SIMS analysis. In most cases, only two
559 MI were analyzed from the same MIA because MI are less abundant in the Solchiaro
560 samples relative to the White Island samples, and the Solchiaro MI are generally smaller.
561 MIA hosted in olivine are either of type 1 (MI containing only glass), type 2 (MI
562 containing glass plus one or more crystals), and type 3 (MI containing glass plus a vapor
563 bubble or plus a vapor bubble and one or more trapped minerals). All of the MIA occur
564 along growth zones or clustered in the core, as in the White Island phenocrysts.

565 **Volatile Contents of White Island MI**

566 We analyzed 124 MI represented by 29 MIA from White Island: 11 MIA are hosted
567 in clinopyroxene, 13 MIA are hosted in plagioclase, and 5 are hosted in orthopyroxene.
568 In most of the MIA, we analyzed < 5 MI, but 8 MI were analyzed from one MIA and 12
569 MI in another MIA, both in plagioclase (Table 2 and Appendix Table 2).

570 Below we first describe the complete range in volatile concentrations, considering all
571 of the MI analyzed, and then we consider the results from individual MIA. Of the 124 MI

572 analyzed, 109 MI are associated with MIA and 15 MI are single MI (only one MI was
573 measured in a single MIA). Of the 109 MI associated with MIA, 101 MI contain only
574 glass (type1), seven MI contain glass plus one or more trapped minerals (type 2), and one
575 MI contain glass plus a sulfide globule (type 4) (Table 2 and Appendix Table 2). It is
576 important to note that 11 MI out of these 109 MI analyzed show irregular shape. $H_2O$
577 contents range from 0.20 to 0.59 wt% (average = 0.37 wt%). One MI contains only 0.13
578 wt% $H_2O$ and this is interpreted to be a degassed (decrepitated?) MI or that the SIMS
579 analysis included both MI (glass) plus a mineral inclusion that, was not recognized during
580 petrographic examination. $H_2O$ concentrations from this study are comparable to those
581 obtained in earlier studies [0.27-0.89 wt% by Rapien et al. (2003), and 0.4-0.8 wt% by
582 Wardell et al. (2001)].

583 Fluorine concentrations range from 163 to 619 ppm (average = 323 ppm) and are
584 generally lower than the 400-800 ppm reported by Rapien et al. (2003).

585 Chlorine concentrations range from 416 to 2,010 ppm (average = 1,020 ppm), a range
586 that is somewhat greaterthan the 500-1,000 ppm reported by Rapien et al. (2003) and
587 comparable to the 1,010-1,770 ppm reported by Wardell et al. (2001). MI hosted in
588 clinopyroxene show the highest Cl content (Fig. 7).

589 Sulfur contents range from 30 to 384 ppm (average = 92 ppm). MI hosted in
590 plagioclase always show S concentrations < 100 ppm, consistent with the absence of
591 sulfide globules in MI hosted in plagioclase, and in agreement with Rapien et al. (2003)
592 and Wardell et al. (2001), who reported S abundances of ≤ 100 ppm in all MI analyzed. It
593 should be noted that White Island is a sulfur-rich volcano, and $SO_2$ emission rates during
594 recent volcanic activity were relatively high (Rose et al., 1986; Wardell et al., 2001). If

595 phenocrysts formed during degassing events of the White Island volcano, it is likely that
596 MI could have recorded S degassing, and would be recognized by variations in sulfur
597 contents of MI. However, we did not observe any correlation between $H_2O$ and S
598 contents, suggesting that other processes, in addition to degassing, likely controlled S
599 abundance in melts trapped by MI.

600 $CO_2$ contents show a wide range (from 39 to 3,508 ppm), with most of the MI having
601 $CO_2$ concentrations <200 ppm. It should be noted that $CO_2$-rich fumaroles were present in
602 the White Island crater during the 1982-1998 activity (Giggenbach and Matsuo, 1991;
603 Giggenbach and Sheppard, 1989; Marty and Giggenbach, 1990; Rose et al., 1986;
604 Tedesco and Toutain, 1991; Wardell et al., 2001), suggesting degassing of a $CO_2$-rich
605 volatile phase from the magma at some unknown depth.

606 For the MIA statistical analysis we have considered only MI that contain only glass
607 (type 1). Additionally, we have not included MI showing irregular shape because
608 irregularly shaped inclusions could represent reentrants, embayments or hourglass MI
609 that became fully enclosed during a later stage of their evolution (Humphreys et al.,
610 2008a; Humphreys et al., 2008b; Welsch et al., 2013). In most of the MIA, $H_2O$ contents
611 are consistent, suggesting that measured $H_2O$ contents are representative of the $H_2O$
612 content of the melt at the time of the trapping (Fig. 7). Most of the MIA show relative
613 standard deviations (RSD) of < 24%, with the exception of one MIA with a somewhat
614 larger RSD of 77% (MIA-27; Table 3 and Appendix Table 2). MIA hosted in
615 orthopyroxene and plagioclase show a narrower range in $H_2O$ contents relative to those
616 hosted in clinopyroxene. For MIA hosted in plagioclase, only one MI (RE-WI-29-E,
617 Table 2) shows an $H_2O$ concentration (0.13 wt%) inconsistent with the other MI in the

618 same MIA (MIA-27, Table 2 and Appendix Table 2). It is worth noting that MIA-27 is an
619 azonal MIA and that the MI may have been trapped over a slightly longer period of time,
620 compared to those in zonal MIAs.

621 Fluorine shows consistent results within all MIA (Fig. 7, Table 3 and Appendix Table
622 2). All MIA show RSD < 24% for F, and several MIA show RSD < 5%. As for $H_2O$, we
623 infer that F concentrations likely represent the F concentration of the melt at the moment
624 of MI trapping.

625 Chlorine contents within all MIA from White Island are also consistent (Fig. 7),
626 suggesting that Cl contents of MI are representative of the melt from which the host
627 phenocrysts were crystallizing. Relative standard deviation for Cl is ≤ 27%, with the
628 exception of one MIA that shows RSD 35% (MIA04; Table 3 and Appendix Table2).

629 Carbon dioxide concentrations were determined for 18 MIA. Ten of the MIA (3
630 hosted in clinopyroxene, 4 hosted in orthopyroxene, and 3 hosted in plagioclase), the
631 RSD was < 50%, and the average concentrations of these eleven MIA is ≤ 200 ppm (Fig.
632 8 Table 3 and Appendix Table 2). Seven of the MIA show much wider variability in $CO_2$
633 content, with RSD of > 100%. MI in these MIA also show higher average $CO_2$ contents
634 compared to MIA with consistent $CO_2$ contents. Both the zonal and the azonal MIAs
635 show similarly large $CO_2$ variability (Fig. 8).

636 Sulfur contents were determined for 26 MIA, and 22 of these show RSD of <33%
637 (Fig. 8, Table 3 and Appendix Table 2). The other 4 MIA show RSD up to 84% and all of
638 these are hosted in clinopyroxene. Sulfur concentrations are generally < 100 ppm for
639 MIA hosted in plagioclase. In one MIA (MIA15, Table2) hosted in clinopyroxene, one
640 type 4 MI (MI containing a sulfide globule, MIA15-I) shows 375 ppm S and the other

641 type 1 (only-glass MI) MI show S concentration as low as 50 ppm (MIA15-D),
642 suggesting that the elevated S contents are due to trapping of immiscible sulfide globules.
643 It is also likely that other MI contain sulfide globules that are either too small to resolve
644 optically, or are obscured by other features in the MI, leading to the relatively wide range
645 in S concentrations obtained by SIMS analysis.

646 In summary, 26 MIA were analyzed for $H_2O$, F, and Cl, and all 26 MIA generally
647 show consistent behavior for these three volatile components. Only one MI in one MIA
648 hosted in plagioclase (MIA-27) shows an $H_2O$ concentration that is inconsistent with the
649 other MI in the MIA. This MI has probably been degassed before or during entrapment
650 because all five of the volatile species measured in this MI have concentrations that are
651 lower relative to the other MI in this MIA. In contrast to $H_2O$, F, and Cl, S concentrations
652 show wide variability in a few MIA, and $CO_2$ concentrations show wide variability in
653 many MIA (Fig. 8). It is important to note that the $CO_2$-$H_2O$ systematics of MI trapped in
654 the same MIA and analyzed here fit trends that are similar to magma degassing paths
655 (Fig. 9). However, MI entrapped in the same MIA (i.e., at the same time and presumably
656 at the same depth or pressure) cannot record a degassing trend because the MIA would
657 have to have formed over a wide range of pressure, which is highly unlikely, if not
658 impossible, based on the petrographic association of the MI in the MIA.
659

660 **Volatile Contents of Solchiaro MIA**

661 As for the White Island sample, we have considered only MI containing only glass
662 (type 1 MI) and showing regular shape. Two MIA hosted in olivine (Table 3 and
663 Appendix Table 2) from Solchiaro were analyzed as part of this study. Three of the MI

664 contained in these two MIA were described previously by Esposito et al. (2011) and
665 eleven new analyses were added to this earlier dataset (Table 2 and Appendix Table 2).
666 Two MI were analyzed several times during different working sessions and in different
667 laboratories (WHOI and Virginia Tech) (Table 2 and 4). As shown in Table 3, the RSD
668 (1 sigma) of one MI (RESC2-O27-MF) that was measured four times is 21% for $CO_2$
669 (718, 529, 501 and 447 ppm), 27% for $H_2O$ (0.99, 1.24, 1.18 and 1.81 wt %; Deposit
670 Item-03), 18% for F, 20% for S, 34% for Cl. It is important to note that the data from the
671 February 2011 session at WHOI are slightly inconsistent with respect to the other
672 measurements on the same MI (RESC2-O27-MF), especially for $CO_2$ and Cl. In
673 particular, the $CO_2$ concentration associated with the WHOI session is higher and $H_2O$, F,
674 S, and Cl are lower relative to the concentrations determined at Virginia Tech (Table 4).
675 We believe this behavior is because the analytical volume for the analysis at WHOI was
676 located closer to the MI/host interface. The different calibration curves used to calculate
677 the concentration of $CO_2$ cannot be the cause of this discrepancy, as is demonstrated by
678 inspection of the calibrations equations listed in Deposit Item-01. Each time the MI was
679 analyzed the SIMS spot was positioned at a different location within the MI, and
680 phenocrysts were polished to remove 1-2 μm of material before each analytical session.
681 These two factors may explain the inconsistency of the data, if the volatiles are
682 distributed heterogeneously within the MI. The other MI that was analyzed three times
683 shows relative 1-sigma errors of 16%, 10%, 3%, 11%, and 24% for $CO_2$, $H_2O$, F, S, and
684 Cl, respectively. These results suggest that the variability observed in some MIA, which
685 is significantly larger than the variability demonstrated by repeated analysis of the same

686 MI, is not the result of the MI being analyzed in different laboratories or during different
687 analytical sessions.

688 Of the two MIA from Solchiaro described here, one MIA contain 2 MI and one MIA
689 contains 3 MI (Table 2 and Appendix Table 2). As was the case for White Island, $H_2O$, F
690 and Cl contents within an MIA are consistent (Fig. 10) and show RSD < 14% for all MIA
691 (Table 3 and Appendix Table 2). S concentrations also show RSD <4% in all MIA. One
692 MIA shows RSD 32% and the other MIA shows RSD 18% for $CO_2$.
693

694 **DISCUSSION**

695 The following discussion is based on the assumption that all of the MI within an MIA
696 were trapped at the *same* time, that is, under the same physical and chemical conditions.
697 Most of the MI analyzed here occur along growth zones (zonal MIA) and represent
698 clearly-defined MIA consisting of primary MI (Bodnar and Student, 2006). It is therefore
699 highly unlikely that the melt that was trapped in the different MI in the zonal MIA could
700 have had different volatile abundances, , unless volatiles were heterogeneously
701 distributed in the bulk melt in the vicinity of the growing crystals.

702 We recognize that melt embayments can develop during crystal growth and
703 subsequently be fully enclosed (e.g., to produce MI) as the crystal continues to grow, as
704 discussed in detail by Welsch et al. (2013) and by Humphreys et al. (2008a) and (2008b).
705 In particular, Humphreys et al. (2008a) state that "…Inclusions trapped during simple
706 crystal growth are typically euhedral (or "negative-crystal" shaped) whereas inclusions
707 trapped in old, corroded cores of partially dissolved crystals are typically highly
708 irregular", suggesting that only irregularly shaped inclusions could represent reentrants,

709 embayments or hourglass MI that became fully enclosed during a later stage of their
710 evolution. While we disagree with this relatively simplistic correlation between MI shape
711 and origin (see, for example, Bodnar et al., 1989), in recognition of the observations by
712 Welsch et al. (2013) and Humphreys et al. (2008a and 2008b), we have restricted our
713 discussion to MIA containing type 1 MI (containing only glass) and showing ovoid,
714 spherical, and negative crystal shape in an attempt to exclude from the dataset any MI
715 that originated as reentrants, embayments or hourglass MI (Appendix Table 2).
716 Establishing the time required to trap MI along a growth zone or in the core of a
717 phenocryst is relevant to the interpretation of data presented here. Bodnar and Student
718 (2006) reported that the amount of time required to trap a 10-μm MI could range from
719 $\sim 10^{-7}$ (~5 sec) to $\sim 10^{3}$ years, based on crystal growth rates in magmas reported by several
720 workers (Bacon, 1989; Dowty, 1980; Tomiya and Takahashi, 2005). Jambon et al. (1992)
721 reported olivine crystal growth rates ranging from $10^{-7}$ to $10^{-6}$ cm $s^{-1}$ for skeletal and
722 dendritic morphology, indicating that a 10-μm MI could be trapped in olivine in ~17
723 minutes to ~3 hours ($\sim 10^{-5}$ to $\sim 10^{-4}$ years).
724 We also assume here that the volatile content of the melt maintains equilibrium with
725 the surrounding PT environment during crystal growth. If the crystal is growing from a
726 volatile-saturated melt, the melt must become super-saturated during crystal growth as
727 non-volatile components are removed from the melt and incorporated into the growing
728 crystal. In the following discussion, we assume that the melt continuously maintains
729 equilibrium, i.e., remains volatile-saturated (but not super-saturated) and, thus, the
730 variability in volatile contents in MIA is not due to trapping of a volatile over-saturated
731 melt during rapid crystal growth, perhaps driven by fast emplacement of deeper, volatile-

732 rich magmas. We note, however, that if the melt does become super-saturated and MI
733 trap aliquots of the super-saturated melt, the $CO_2$-$H_2O$ systematics of the MIA would
734 likely define a trend represented by relatively large variation of $H_2O$ vs. a relatively
735 narrow range of $CO_2$, owing to the faster diffusion of H (e.g., $H_2O$ and $OH^-$) relative to C
736 (e.g., $CO_2$ and $CO_3^{2-}$) in silicate melts (Zhang and Ni, 2010).

737 In this study, we found that concentrations of $H_2O$, F, and Cl are in most cases
738 consistent within a single MIA, whereas S and especially $CO_2$ contents show much more
739 variability. Thus, the volatile concentrations of the majority of the MIA analyzed in this
740 study are consistent, within analytical uncertainty, and likely represent the volatile budget
741 of the melt from which the phenocrysts were precipitating. Below we discuss the low
742 $H_2O$ concentration of MIA hosted in phenocrysts from White Island and consider
743 possible explanations for those MIA that do not show consistent behavior for $CO_2$.
744

745 **Water content of White Island MI**

746 At first glance, the low water contents (~0.37 wt.%) determined for MI from White
747 Island might be cause for concern as these values are somewhat less than would be
748 expected in arc volcano magmas, which typically range from ~1 to 6 wt% $H_2O$ (Wallace,
749 2005). We consider whether the relatively consistent $H_2O$ contents of MIA examined
750 here represent the $H_2O$ content of the trapped melt, or if they could have been modified
751 after trapping and still show consistent concentrations within an MIA. It is well known
752 that various post-entrapment processes can affect the volatile concentrations of MI. For
753 instance, Gaetani et al. (2012) reported that H in MI in olivine can re-equilibrate with the
754 surrounding environment in a few hours (see Figure 2 in their study), owing to the fast

755 diffusion of H through olivine at magmatic temperatures. More recently, Bucholz et al.
756 (2013) reported that volatile-rich MI hosted in olivine undergo re-equilibration with the
757 surrounding melt in ~10 hours at 1250ºC and in a few days at 1100ºC. As reported above,
758 $H_2O$-loss from MI produces a $CO_2$-$H_2O$ trend similar to the trend produced by magma
759 degassing. In fact, $H_2O$ loss decreases the internal pressure in the MI, leading to the
760 formation or expansion of a vapor bubble, and concomitant decrease in the $CO_2$
761 concentration in the melt (Bucholz et al., 2013; Gaetani et al., 2012). Similarly, Severs et
762 al. (2007) reported that, while MI hosted in quartz do not experience significant water
763 loss after 12 hours of reheating, after 63 days at 800ºC the MI may lose as much as 75%
764 of the $H_2O$ that was in the melt at the time of trapping. Both of these processes would
765 likely produce MIA with inconsistent $H_2O$ contents, depending on the location of the MI
766 within the phenocryst (relative to the rim) and the MI size.
767 Low water content melts associated with subduction zone magmatism, such as those
768 found in this study (0.37 wt% average), are rare (Sisson and Bronto, 1998; Sisson and
769 Layne, 1993; Wallace, 2005). In order to assess whether the low water contents are
770 consistent with the magma chemistry, we performed calculations using the plagioclase-
771 melt hygrometers developed by Putirka (2005) and Lange et al. (2009). For the
772 calculations, we used the average composition of plagioclase reported by Rapien et al.
773 (2003), and average composition of White Island MI from the 1986 eruption reported by
774 Rapien et al. (2003). For the Lange et al. (2009) hygrometer, the input temperature
775 ranged from 1043°C to 1210°C, based on the two-pyroxene thermometer (Brey and
776 Köhler, 1990; Putirka, 2008) and MI homogenization temperatures (Rapien et al, 2003),
777 respectively. The average $H_2O$ concentration of White Island MI from this study is 0.37

778 wt% and is consistent with results predicted by the plagioclase-melt hygrometer of
779 Putirka (2005) and Lange et al. (2009). In particular, the plagioclase-melt hygrometer of
780 Lange et al. (2009) predicts that the $H_2O$ content of the melt would be 0.37 wt% at
781 1190°C and 200 MPa, or at 1167°C and 10 MPa. The measured low $H_2O$ contents are
782 thus consistent with the plagioclase-silicate melt system at the temperature obtained from
783 heating experiments of MI. However, the temperature range that is consistent with an
784 $H_2O$ content of 0.37 wt.% is significantly higher than the temperature obtained using the
785 two-pyroxene thermometer.

786 The plagioclase-melt hygrometer of Putirka (2005) predicts that the melt would
787 contain 0.37 wt% $H_2O$ at 1088°C and 200 MPa. This temperature is close to the
788 temperature predicted by the two-pyroxene thermometer (but less than the measured MI
789 homogenization temperatures or the temperatures predicted by the model of Lange et al.
790 (2009)). The water content of White Island melts predicted by the plagioclase-silicate
791 melt hygrometer suggests that the low $H_2O$ contents (~ 0.37 wt%) obtained are not
792 unrealistic, and the temperature and pressure conditions required for this water content
793 are within a reasonable range for the White Island system.

794 If the melt that was trapped as MI was $H_2O$ saturated, the low-$H_2O$ concentrations
795 indicate that the MI were trapped at low pressure (i.e., in a shallow magma chamber).
796 This is in agreement with geophysical data that indicate that the 1977 eruption at White
797 Island originated from a very shallow level (<2 km) (Clark and Otway, 1989; Houghton
798 and Nairn, 1989; Sherburn et al., 1998). In fact, at volatile saturation, the pressure
799 estimated from the volatile data from consistent MIA is $\leq$ 32 MPa, calculated using the
800 $H_2O$-$CO_2$-silicate melt solubility model by Papale et al. (2006), with FeO = 0.8 x $FeO_{tot}$,

1100 ˚C, and the average MI major element composition reported by Rapien et al. (2003). Inferred depths of formation based on the calculated pressures are in agreement with geophysical data (Clark and Cole, 1989). Considering the MIA showing the least variability for $CO_2$ (MIA-33, RSD 7%), the calculated pressures of formation range from 21.5 to 25.0 MPa using the Papale et al. model and the parameters listed above. We thus conclude that the $H_2O$ concentrations of White island MI, while less than those of most arc-related magmas, are consistent with other geochemical and geophysical data and representative of the melt at the moment of trapping.

**Why does the concentration of carbon dioxide show large variability?**

Of the five volatile components that were measured, the one that showed the least consistency was $CO_2$, and the variability is most pronounced for MIA hosted in plagioclase. Various processes may be responsible for the observed $CO_2$ variability including (1) Carbon contamination of the sample, (2) MI within an MIA trapped a volatile saturated melt over a wide pressure (depth) range, (3) $CO_2$ was heterogeneously distributed in the melt before the MIA was trapped, (4) Post entrapment diffusive re-equilibration, (5) Post-entrapment crystallization on the MI/host interface, and (6) heterogeneous distribution of $CO_2$ in the MI. Below we consider each of these possible explanations.

*Carbon contamination*

One possible explanation of the variable $CO_2$ concentrations of MI within an MIA is carbon contamination on the surface of the sample or other analytical errors, as suggested by the large standard deviations of some $CO_2$ analyses. In some cases, the $CO_2$

824 concentration significantly decreases from the beginning to the end of the analysis,
825 indicating that the near-surface material contains more $CO_2$ (or carbon) compared to
826 material that is deeper beneath the surface. As stated in the Analytical Methods section,
827 we discarded those analyses showing real time C heterogeneity, possibly related to
828 particles on the surface of the sample. To test the likelihood that C contamination is the
829 cause of the widely variable $CO_2$ contents observed for some MIA, we examined the
830 variability in $CO_2$ contents of those MI that were analyzed multiple times (with additional
831 polishing between analyses to remove more surface material for some MI) (Fig. 11).
832 Only one MI out of 24 that were analyzed two or more times showed inconsistent $CO_2$
833 concentrations, suggesting that C contamination is not the cause of the relatively
834 widespread variability in $CO_2$ concentrations observed in some MIA. As a further test,
835 we performed depth profiles to test for homogeneity of $CO_2$ with depth in an MI. As
836 shown on Fig. 12, the initial (shallow) part of the $CO_2$ profile shows erratic behavior, and
837 is mainly characterized by elevated $CO_2$ contents. It is important to note that this
838 anomalous behavior is more significant for MI hosted in plagioclase, which is consistent
839 with the more pronounced variability of $CO_2$ in MIA hosted in plagioclase. $CO_2$ depth
840 profiling of glass standards and MI hosted in pyroxene and olivine does not show such
841 strong enrichment of $CO_2$ in the initial (shallow) near-surface portion of the sample (Fig.
842 12). In plagioclase, we noticed that the erratic $CO_2$ profile sometimes persists to ~2 μm
843 below the sample surface. Note that the depth at which the contamination signal
844 disappears does not necessarily correspond to the true depth in the case where C
845 contamination is due to particles residing on the sample surface. In fact, the sputtering
846 rate on C-rich particles can be as much as 10 times slower than the sputtering rate on

847 silicate glass. As such, the carbon signal will continue as sputtering of the underlying
848 silicate glass begins and continues. Moreover, the initial roughness of the sample surface
849 controls depth resolution using SIMS (Hunter, 2009). If the C contamination is mainly
850 due to sample preparation, it is remarkable that MI in plagioclase crystals are more
851 affected than MI in other host minerals. In fact, plagioclase, clinopyroxene,
852 orthopyroxene, and olivine were all mounted in the same indium mounts and the sample
853 preparation procedures were the same for each of these host phases. Also, glass standards
854 were mounted, prepared, and cleaned using the same method as for the last mount
855 analyzed for this study.

856 To test if carbon contamination is introduced by the sample preparation method used
857 at Virginia Tech, as collected (unprepared) crystals from White Island were prepared and
858 analyzed by coauthor Shimizu at WHOI. The crystals were mounted, polished and
859 analyzed following the WHOI procedure for volatile analysis of MI (Table 5). A depth
860 profile obtained on one of the MI (analyses 860210-MI-8 and MI-8-2 in MI-8) analyzed
861 at WHOI shows that the $CO_2$ content of the MI obtained from the early (the shallowest
862 glass) part of the depth profile was 608 ppm, but the concentration obtained from the later
863 (the deepest glass) part of the depth profile in the same MI was 282 ppm (Deposit Item-
864 04). This variation in $CO_2$ content, observed in a single MI, is similar to the range in $CO_2$
865 content observed in other White Island MI. It is important to note that analyses 860210-
866 MI-8 and MI8-2 were done on the same spot and the spot was close to the MI/host
867 interface. The results obtained for 860210-MI-8 and MI8-2 are consistent with the
868 interpretation that C contamination is present at the MI/host interface, or that the glass
869 near the interface is naturally enriched in $CO_2$, but it is not possible to determine which of

these causes is more likely. During this analytical session at WHOI, only a single MI from each MIA was analyzed, and MI were hosted in clinopyroxene or in orthopyroxene but not in plagioclase.

*Trapping of volatile-saturated melt at various pressure*

Various studies have invoked entrapment of MI over a wide range of pressure as a result of sinking of crystals in a magma chamber (Anderson et al., 2000), or phenocrysts growing at different depths in the magma plumbing system during the ascent of magma batches (Métrich and Wallace, 2008 and references therein). The individual MI in a zonal MIA studied here could not have been trapped over a significant range of pressure because petrographic evidence documents that the MI were all trapped simultaneously. Moreover, the homogeneous major element compositions of MI and the unzoned nature of the clinopyroxenes do not support entrapment over a wide range of pressure because the composition of the melt and the phenocryst should reflect these changing $P(T)$ growth conditions, and the melt and crystal compositions do not vary.

*Heterogeneous distribution of carbon dioxide in the bulk melt*

Another possible explanation for the range in $CO_2$ concentration is that the melt surrounding the growing phenocryst is compositionally inhomogeneous. A melt in which $CO_2$ is heterogeneously distributed could possibly be produced if a $CO_2$-rich magma rapidly ascended to shallow depth, generating a $CO_2$ over-saturated melt. This process could lead to a wide range in $CO_2$ contents of the MI within an MIA – in this case the lowest $CO_2$ concentration would most closely represent the true composition of the original melt at the depth of MI trapping, with all higher values representing the $CO_2$-oversaturated melt. Studies on dynamics of bubble formation suggest that overpressure

893 required for bubble nucleation varies with melt composition (Mangan et al., 2004;
894 Sparks, 1978). In particular, Mangan et al. (2004) argued that supersaturation pressures
895 are much lower for dacitic melts (35 ±5 MPa) than for rhyolitic melts (up to 350 MPa) in
896 crystal-free melts that do not have solid phases to serve as sites of bubble nucleation. The
897 composition of White Island MI considered in this study is dacitic and contained crystals
898 at the time of MI formation, and likely the melt was not.

899 Another possibility to explain the $CO_2$ variability in an MIA is heterogeneous
900 distribution of $CO_2$ within individual MI. As noted by Steele-MacInnis et al. (2011), if an
901 $H_2O$-$CO_2$-saturated melt inclusion experiences post-entrapment crystallization (PEC) on
902 the walls, $CO_2$ (and little $H_2O$) will be lost from the melt as crystallization proceeds.
903 Because crystallization necessarily occurs at the melt/crystal interface, a $CO_2$-enriched
904 zone may form at the interface if the $CO_2$ cannot diffuse into the vapor bubble before the
905 MI is quenched. The presence of a volatile-enriched rim in MI is supported by results
906 from Le Voyer et al. (2012), who analyzed volatile concentrations of MI by nano-SIMS
907 and observed that MI are zoned with respect to H and F abundances. Similarly, Helo et
908 al. (2011) reported that some MI in plagioclase show $CO_2$ concentrations that vary with
909 depth in the MI (see Supplementary Figure S5 of their study). In addition, Mormone et al.
910 (2011) mapped the $CO_2$ and $H_2O$ distribution in MI using Focal-Plane-Array applied to
911 Fourier Transform Infrared spectroscopy and documented that $H_2O$ and $CO_2$ can be
912 heterogeneously distributed within MI (see $CO_2$ distribution close to the bubble in their
913 Fig. 4c). However, Mormone et al. (2011) argue that the depletion of $CO_2$ and $H_2O$ at the
914 rim is an artifact of the MI geometry changing at the edge. In the present study, depth
915 profiling of unexposed MI in plagioclase by SIMS shows that $CO_2$ is strongly enriched

916 near the host/MI interface (Fig. 13). The enrichment at host/MI interface can be due to C
917 contamination, as discussed above. But, because we have not exposed the MI on the
918 surface, we can rule out C contamination unless sub-microscopic fractures extend from
919 the surface to the MI at depth and provide conduits for C to enter the sample.

920 Results presented above suggest that the $CO_2$ content determined for an MI may
921 depend on the specific location within the MI that is analyzed. For instance, if during
922 polishing the exposed surface that is produced for SIMS analysis is close to the
923 MI/crystal interface that was present before the host was removed to expose the MI, the
924 analysis would be conducted on glass that was close to the host/MI interface before the
925 host was removed by polishing. In this case, the $CO_2$ content could be higher than that
926 which would be obtained if more MI material had been removed during polishing to
927 expose glass located more distant from the MI/crystal interface. The measured $CO_2$
928 concentration may also depend on the MI morphology, as an MI with irregular walls
929 could result (after polishing) in a flat glass with variably volatile-enriched portions of the
930 MI exposed at the surface. It is important to note that FTIR may provide better results
931 compared to SIMS analysis if the $CO_2$ variability is due to heterogeneous distribution
932 within MI, because FTIR samples a larger portion of the total MI in most cases.

933 *Post-entrapment diffusive re-equilibration*

934 Another possible explanation for the highly variable $CO_2$ concentrations recorded by
935 some MIA is post-entrapment re-equilibration involving C diffusion into or out of the
936 bubble-free MI. However, we are unaware of any studies that document that $CO_2$
937 concentrations of MI can be affected by diffusion. [We acknowledge, however, that the
938 $CO_2$ content of the glass phase in the MI may be affected by H diffusion, as shown by

939 Gaetani et al. (2012)] Conversely, several studies have documented an inverse correlation
940 between crystallization indicator and $CO_2$ concentration based on MI (Benjamin et al.,
941 2007; Esposito et al., 2011; Wade et al., 2006; Wallace et al., 1999), suggesting that in
942 these studies $CO_2$ has not diffused into or out of the MI following trapping.

943 **Summary of Uncertainties Associated with Volatile Analysis of MI using Secondary**
944 **Ion Mass Spectrometry**

945 In this study we have measured the concentrations of $CO_2$, $H_2O$, Cl, S, and F in 29 Melt
946 Inclusion Assemblages (MIA) from the White Island volcano in New Zealand and from
947 the Solchiaro eruption on the Island of Procida (Italy) by Secondary Ion Mass
948 Spectrometry (SIMS). All of the MI within a given MIA were trapped at the same time,
949 and thus all (presumably) trapped a melt of the same composition and at the same PT
950 conditions. Thus, because all of the MI within the MIA have the same volatile
951 concentrations, and any apparent variations in volatile abundances within the MIA
952 represent the uncertainty in volatile determination. Moreover, because the samples were
953 prepared and analyses were conducted in two different laboratories, with similar results,
954 variations in volatile abundances obtained in this study cannot be related to within-
955 laboratory procedures. As such, we suggest that the uncertainties obtained in this study
956 are generally applicable to all analyses of volatiles in MI conducted by SIMS, and thus
957 represent the precision with which volatile contents can be estimated. Below we
958 summarize these uncertainties.

959 • The Relative Standard Deviation (RSD) for $H_2O$ varies from 0% to 23% with one
960 outlier at 77%, with a median RSD of 8% and mean of 13% (Fig. 14). The 1
961 sigma variation in the slope of calibration curves for $H_2O$ is 20%. Thus, the

962 variation in $H_2O$ concentration obtained by SIMS is comparable to the variation
963 in calibration curves, and most of the uncertainty is likely related to
964 instrumental fluctuations. These data suggest that the $H_2O$ concentration of MI
965 determined by SIMS has an uncertainty of ~10-15%.

966 • The Relative Standard Deviation (RSD) for F varies from 1% to 23%, with a
967 median RSD of 8% and mean of ~10% (Fig. 14). The 1-sigma variation in the
968 slope of calibration curves for F is 12%. Thus, the variation in F concentration
969 obtained by SIMS is comparable to the variation in calibration curves, and most
970 of the uncertainty is likely related to instrumental fluctuations. These data
971 suggest that, in most of the cases, the F concentration of MI determined by
972 SIMS has an uncertainty ~10%.

973 • The Relative Standard Deviation (RSD) for Cl varies from 1% to 35%, with a
974 median RSD of 10% and mean of 13% (Fig. 14). The 1 sigma variation in the
975 slope of calibration curves for Cl is ~11%. Thus, the variation in Cl
976 concentration obtained by SIMS is comparable to the variation in calibration
977 curves, and most of the uncertainty is likely related to instrumental fluctuations.
978 These data suggest that , in most of the cases, the Cl concentration of MI
979 determined by SIMS has an uncertainty of ~10-15%.

980 • The Relative Standard Deviation (RSD) for S varies from ~0% to 84%, with a
981 median RSD of 16% and mean of ~22% (Fig. 14). The 1 sigma variation in the
982 slope of calibration curves for S is ~9%. Thus, unlike for $H_2O$, Cl and F, the
983 variation in S concentration obtained by SIMS is significantly larger than the
984 variation in calibration curves, and some of the uncertainty is likely related to

non-instrumental factors, possibly including the trapping of submicroscopic sulfide blebs in the MI or heterogeneous distribution of S within the MI. These data suggest that the S concentration of MI determined by SIMS has an uncertainty of ~15-25%.

- The Relative Standard Deviation (RSD) for $CO_2$ shows much more variation than the other four volatile components considered, and ranges from 7% to 137%, with a median RSD of 52% and mean of 65% (Fig. 14). The 1 sigma variation in the slope of calibration curves for $CO_2$ is ~12%. Thus, similar to S, the variation in $CO_2$ concentration obtained by SIMS is significantly larger than the variation in calibration curves, and some of the uncertainty is likely related to non-instrumental factors, possibly including the heterogeneous distribution of $CO_2$ within the MI. These data suggest that the $CO_2$ concentration of MI determined by SIMS has an uncertainty of ~60%.

## SUMMARY

Analysis of groups of melt inclusions that were all trapped at the same time (Melt Inclusion Assemblages, or MIA) and at the same pressure (depth) in an evolving magmatic system show consistent results for $H_2O$, F, Cl and, to a lesser extent, S contents, suggesting that the MI trapped a representative sample of the melt that the host crystal was growing from and preserved the volatile composition during continued phenocryst growth, eventual eruption onto the surface, and quenching. Conversely, $CO_2$ contents show much more variability within MIA, although many MIA do show relatively consistent results for $CO_2$. Several processes could potentially lead to the observed $CO_2$ variability in MIA, but it is not possible to determine with certainty which

process or processes are responsible. And, although the results presented here do not identify the cause of the variability, it is clear that the measured $CO_2$ contents of MI that were all trapped at the same time sometimes show large variability. Importantly, $CO_2$-$H_2O$ systematics of MIA that show variability in $CO_2$ often define trends that are similar to trends that would be produced by an ascending, volatile-saturated magma undergoing degassing (Fig. 9).

It is critical that workers study MIA whenever possible to test the reliability of MI. In fact, if bubble-free MI within a zonal MIA all record the same volatile concentrations, strong and defensible evidence is provided that the measured volatile concentration is reliable and represents the concentration in the melt that was trapped at depth. If $CO_2$ and $H_2O$ concentrations in individual MIA define a degassing path, one can be reasonably confident that the volatile trend does indeed reflect a degassing path. Conversely, a $CO_2$ vs. $H_2O$ trend based on analyses of individual MI from numerous, randomly-selected phenocrysts with an unknown temporal or genetic relationship between MI may represent trapping along a degassing path, but proving such may be difficult in the absence of other supporting geochemical data.

We suggest that the uncertainties estimated in this study represent the precision of volatile determinations of MI by SIMS under normal operating conditions. As such, any trends or geochemical interpretations based on variations with magnitudes that are equal to, or less than, these uncertainties should be viewed with caution, as the variability may simply represent the natural variability associated with instrumental factors (including location of the primary beam within the MI), as well as the characteristics of the MI

being analyzed, such as shape and the proximity of volume being sampled to the MI/host interface.

## ACKNOWLEDGEMENTS

The authors would like to thank J. D. Rimstidt, R. J. Tracy, B. De Vivo, A. Lima, and M. Steele-McInnis for valuable discussions and comments that helped to improve this manuscript. We sincerely thank R. Lange for helping with calculations using the plagioclase-silicate melt hygrometer. In addition, we thank P. Wallace, A. Costa and other two anonymous reviewers to have greatly improved this manuscript. R. Esposito thanks N. Jackson for helping with statistical analysis to calculate SIMS calibration curves. This study has been supported by the National Science Foundation under grant no. EAR-1019770.

## REFERENCES CITED

Alessio, M., Allegri, L., Azzi, C., Calderoni, G., Cortesi, C., Improta, S., and Petrone, V. (1989) $^{14}C$ tephrochronology with different fractions of Paleosol humic matter at Procida Island, Italy. Radiocarbon, 31, 664-671.

Anderson, A.T., and Brown, G.G. (1993) CO 2 contents and formation pressures of some Kilauean melt inclusions. American Mineralogist, 78(7-8), 794-803.

Anderson, A.T., Davis, A.M., and Lu, F.Q. (2000) Evolution of Bishop Tuff rhyolitic magma based on melt and magnetite inclusions and zoned phenocrysts. Journal of Petrology, 41(3), 449-473.

Anderson, A.T., Newman, S., Williams, S.N., Druitt, T.H., Skirius, C., and Stolper, E. (1989) H2O, CO2, CI, and gas in Plinian and ash-flow Bishop rhyolite. Geology, 17(3), 221-225.

Asimow, P.D., and Ghiorso, M.S. (1998) Algorithmic modifications extending MELTS to calculate subsolidus phase relations. American Mineralogist, 83(9-10), 1127-1132.

Audétat, A., and Lowenstern, J.B. (2014) 13.6 - Melt Inclusions. In H.D. Holland, and K.K. Turekian, Eds. Treatise on Geochemistry (Second Edition), p. 143-173. Elsevier, Oxford.

1060 Bacon, C.R. (1989) Crystallization of accessory phases in magmas by local saturation
1061 adjacent to phenocrysts. Geochimica Et Cosmochimica Acta, 53(5), 1055-1066.
1062 Baker, D. (2008) The fidelity of melt inclusions as records of melt composition.
1063 Contributions to Mineralogy and Petrology, 156(3), 377-395.
1064 Benjamin, E.R., Plank, T., Wade, J.A., Kelley, K.A., Hauri, E.H., and Alvarado, G.E.
1065 (2007) High water contents in basaltic magmas from Irazu Volcano, Costa Rica.
1066 Journal of Volcanology and Geothermal Research, 168(1-4), 68-92.
1067 Bodnar, R.J. (2003) Introduction to fluid inclusions. In I. Samson, A. Anderson , and D.
1068 Marshall, Eds. Fluid Inclusions: Analysis and Interpretation, Short Course, p. 1-8.
1069 Mineralogical Association of Canada.
1070 Bodnar, R.J., Binns, P.R., and Hall, D.L. (1989) Synthetic fluid inclusions - VI.
1071 Quantitative evaluation of the decrepitation behaviour of fluid inclusions in quartz
1072 at one atmosphere confining pressure. Journal of Metamorphic Geology, 7(2),
1073 229-242.
1074 Bodnar, R.J., and Student, J.J. (2006) Melt inclusions in plutonic rocks: Petrography and
1075 microthermometry. Melt Inclusions in Plutonic Rocks, 36(Short Course ), 1-25.
1076 Brey, G.P., and Köhler, T. (1990) Geothermobarometry in Four-phase Lherzolites II.
1077 New Thermobarometers, and Practical Assessment of Existing
1078 Thermobarometers. Journal of Petrology, 31(6), 1353-1378.
1079 Bucholz, C.E., Gaetani, G.A., Behn, M.D., and Shimizu, N. (2013) Post-entrapment
1080 modification of volatiles and oxygen fugacity in olivine-hosted melt inclusions.
1081 Earth and Planetary Science Letters, 374(0), 145-155.
1082 Cecchetti, A., Fulignati, P., Marianelli, P., Proto, N., Sbrana, A. (2001) The feeding
1083 system of Campi Flegrei. Insights from melt and fluid inclusions on Ignimbrite
1084 Campana, Solchiaro and Minopoli eruptions. GNV-INGV Meeting, Abstracts vol,
1085 p. 190–191, Rome, Italy.
1086 Clark, R.H., and Cole, J.W. (1989) Volcanic monitoring and surveillance at White Island
1087 before the 1976-82 eruption sequence. In B.F. Houghton, and I.A. Nairn, Eds.
1088 New Zealand Geological Survey, Wellington.
1089 Clark, R.H., and Otway, P.M. (1989) Deformation monitoring associated with the 1976–
1090 82 White Island eruptive sequence. In B.F. Houghton, and I.A. Nairn, Eds. The
1091 1976–82 Eruption Sequence at White Island Volcano (Whakaari), Bay of Plenty,
1092 New Zealand, 103, p. 69-84. New Zealand Geological Survey Bulletin.
1093 Cole, J.W., Thordarson, T., and Burt, R.M. (2000) Magma Origin and Evolution of White
1094 Island (Whakaari) Volcano, Bay of Plenty, New Zealand. Journal of Petrology,
1095 41(6), 867-895.
1096 D'Antonio, M., Civetta, L., and Di Girolamo, P. (1999) Mantle source heterogeneity in
1097 the Campanian Region (South Italy) as inferred from geochemical and isotopic
1098 features of mafic volcanic rocks with shoshonitic affinity. . Mineralogy and
1099 Petrology 67, 163–192.
1100 Danyushevsky, L.V., Leslie, R.A.J., Crawford, A.J., Durance, P., Niu, Y., Herzberg, C.,
1101 and Wilson, M. (2004) Melt inclusions in primitive olivine phenocrysts; the role
1102 of localized reaction processes in the origin of anomalous compositions. Journal
1103 of Petrology, 45(12), 2531-2553.
1104 Danyushevsky, L.V., McNeill, A.W., and Sobolev, A.V. (2002) Experimental and
1105 petrological studies of melt inclusions in phenocrysts from mantle-derived

magmas: an overview of techniques, advantages and complications. Chemical Geology, 183(1-4), 5-24.

De Astis, G., Piochi, M., and Pappalardo, L. (2004) Procida Volcanic History: new insights in the evolution of the Phlegraean Volcanic District (Campania, Italy). Bulletin of Volcanology, 66, 622-641.

De Vivo, B., and Bodnar, R.J. (2003) Melt inclusions in volcanic systems. Elsevier Sciences, Amsterdam.

Di Girolamo, P., Ghiara, M.R., Lirer, Munno, R., Rolandi, G., and Stanzione, D. (1984) Vulcanologia e petrologia dei Campi Flegreei. Volcanology and petrology of Phlegraean Fields. Bollettino della Società Geologica Italiana 103, 349-413.

Dowty, E. (1980) Crystal growth and nucleation theory and the numerical simulation of igneous crystallization. In R.B. Hargraves, Ed. Princeton Univ. Press, Princeton.

Esposito, R., Bodnar, R.J., Danyushevsky, L., De Vivo, B., Fedele, L., Hunter, J., Lima, A., and Shimizu, N. (2011) Volatile Evolution of Magma Associated with the Solchiaro Eruption in the Phlegrean Volcanic District (Italy). Journal of Petrology, 52(12), 2431-2460.

Faure, F., and Schiano, P. (2005) Experimental investigation of equilibration conditions during forsterite growth and melt inclusion formation. Earth and Planetary Science Letters, 236(3–4), 882-898.

Gaetani, G.A., O'Leary, J.A., Shimizu, N., Bucholz, C.E., and Newville, M. (2012) Rapid reequilibration of H2O and oxygen fugacity in olivine-hosted melt inclusions. Geology, 40(10), 915-918.

Gaetani, G.A., and Watson, E.B. (2002) Modeling the major-element evolution of olivine-hosted melt inclusions. Chemical Geology, 183(1–4), 25-41.

Ghiorso, M.S., and Sack, R.O. (1995) Chemical mass transfer in magmatic processes IV. A revised and internally consistent thermodynamic model for the interpolation and extrapolation of liquid-solid equilibria in magmatic systems at elevated temperatures and pressures. Contributions to Mineralogy and Petrology, 119(2-3), 197-212.

Giggenbach, W.F., and Matsuo, S. (1991) Evaluation of results from Second and Third IAVCEI Field Workshops on Volcanic Gases, Mt Usu, Japan, and White Island, New Zealand. Applied Geochemistry, 6(2), 125-141.

Giggenbach, W.F., and Sheppard, D.S. (1989) Variations in the temperature and chemistry of White Island fumarole discharges 1972–1985. In B.F. Houghton, and I.A. Nairn, Eds. The 1976–82 Eruption Sequence at White Island Volcano (Whakaari), Bay of Plenty, New Zealand, 103, p. 119-126, Rotorua.

Goldstein, D.J., and Reynolds, D.C. (1994) Systematics of fluid inclusions in diagenetic minerals. SEPM Short Course Notes 31, 199.

Graham, I.J., and Cole, J.W. (1991) Petrogenesis of andesites and dacites of White Island volcano, Bay of Plenty, New Zealand, in the light of new geochemical and isotopic data. New Zealand Journal of Geology and Geophysics, 34(3), 303-315.

Graham, I.J., Cole, J.W., Briggs, R.M., Gamble, J.A., and Smith, I.E.M. (1995) Petrology and petrogenesis of volcanic rocks from the Taupo Volcanic Zone: a review. Journal of Volcanology and Geothermal Research, 68(1–3), 59-87.

Hauri, E. (2002) SIMS analysis of volatiles in silicate glasses, 2: isotopes and abundances in Hawaiian melt inclusions. Chemical Geology, 183(1-4), 115-141.

Helo, C., Longpre, M.-A., Shimizu, N., Clague, D.A., and Stix, J. (2011) Explosive eruptions at mid-ocean ridges driven by CO2-rich magmas. Nature Geosci, 4(4), 260-263.

Houghton, B.F., and Nairn, I.A. (1989) A model for the 1976–1982 phreatomagmatic and strombolian eruption sequence at White Island volcano, New Zealand. In B.F. Houghton, and I.A. Nairn, Eds. The 1976–82 Eruption Sequence at White Island volcano (Whakaari), Bay of Plenty, New Zealand, 103, p. 127-136. New Zealand Geological Survey Bulletin.

Humphreys, M.C.S., Blundy, J.D., and Sparks, R.S.J. (2008a) Shallow-level decompression crystallisation and deep magma supply at Shiveluch Volcano. Contributions to Mineralogy and Petrology, 155(1), 45-61.

Humphreys, M.C.S., Menand, T., Blundy, J.D., and Klimm, K. (2008b) Magma ascent rates in explosive eruptions: Constraints from H2O diffusion in melt inclusions. Earth and Planetary Science Letters, 270(1–2), 25-40.

Hunter, J.L. (2009) Improving Depth Profile Measurements of Natural Materials: Lessons Learned from Electronic Materials Depth-Profiling. In M. Fayek, Ed. Secondary Ion Mass Spectrometry in the Earth Sciences:

Gleaning the Big Picture from a Small Spot, 41, p. 133-148. Mineralogical Association of Canada, Toronto.

Isacks, B., Oliver, J., and Sykes, L.R. (1968) Seismology and the new global tectonics. Journal of Geophysical Research, 73(18), 5855-5899.

Jambon, A., Lussiez, P., Clocchiatti, R., Weisz, J., and Hernandez, J. (1992) Olivine Growth-Rates in a Tholeiitic Basalt - an Experimental-Study of Melt Inclusions in Plagioclase. Chemical Geology, 96(3-4), 277-287.

Kamenetsky, V.S., Pompilio, M., Métrich, N., Sobolev, A.V., Kuzmin, D.V., and Thomas, R. (2007) Arrival of extremely volatile-rich high-Mg magmas changes explosivity of Mount Etna. Geology, 35(3), 255-258.

Kent, A.J.R. (2008) Melt inclusions in basaltic and related volcanic rocks. In K.D. Putirka, and F.J. Tepley, III, Eds. MInerals, Inclusions and Volcanic Processes, 69, p. 273-331. The Mineralogical Society of America.

Kress, V.C., and Ghiorso, M.S. (2004) Thermodynamic modeling of post-entrapment crystallization in igneous phases. Journal of Volcanology and Geothermal Research, 137(4), 247-260.

Lange, R.A., Frey, H.M., and Hector, J. (2009) A thermodynamic model for the plagioclase-liquid hygrometer/thermometer. American Mineralogist, 94(4), 494-506.

Le Voyer, M., Newcombe, M., Stolper, E., and Eiler, J.M. (2012) The nanoSIMS as a Tool to Study Zonation Around/in Melt Inclusions. Mineralogical Magazine, 76(6), 1984.

Lirer, L., Rolandi, G., and Rubin, M. (1991) $^{14}C$ age of the "Museum Breccia" (Campi Flegrei) and its relevance for the origin of the Campanian Ignimbrite. Journal of Volcanology and Geothermal Research, 48(1-2), 223-227.

Lowenstern, J.B. (1995) Applications of silicate-melt inclusions to the study of magmatic volatiles. Short Course Handbook, 23, 71-99.

Lowenstern, J.B., and Pitcher, B.W. (2013) Analysis of H2O in silicate glass using attenuated total reflectance (ATR) micro-FTIR spectroscopy. American Mineralogist, 98(10), 1660-1668.

Luhr, J. (2001) Glass inclusions and melt volatile contents at Parícutin Volcano, Mexico. Contributions to Mineralogy and Petrology, 142(3), 261-283.

Mangan, M., Mastin, L., and Sisson, T. (2004) Gas evolution in eruptive conduits: combining insights from high temperature and pressure decompression experiments with steady-state flow modeling. Journal of Volcanology and Geothermal Research, 129(1–3), 23-36.

Marty, B., and Giggenbach, W.F. (1990) Major and Rare Gases at White Island Volcano, New Zealand: Origin and Flux of Volatiles. Geophysical Research Letters, 17(3), 247-250.

Métrich, N., and Wallace, P.J. (2008) Volatile abundances in basaltic magmas and their degassing paths tracked by melt inclusions. In K.D. Putirka, and F.J. Tepley, III, Eds. MInerals, Inclusions and Volcanic Processes, 69, p. 363-402. The Mineralogical Society of America.

Moore, L., Esposito, R., Gazel, E., Tuohy, R., Wallace, P., and Bodnar, R.J. (2013) Hawaiian melt inclusion "shrinkage bubbles" contain dense $CO_2$ vapor: Implications for inferred $CO_2$ contents of trapped melts. European Current Research on Fluid Inclusions (ECROFI-XXII), Abstract Book, p. 199-200, Antalya, Turkey.

Mormone, A., Piochi, M., Bellatreccia, F., De Astis, G., Moretti, R., Della Ventura, G., Cavallo, A., and Mangiacapra, A. (2011) A $CO_2$-rich magma source beneath the Phlegraean Volcanic District (Southern Italy): Evidence from a melt inclusion study. Chemical Geology, 287(1-2), 66-80.

Newman, S., and Lowenstern, J.B. (2002) VolatileCalc; a silicate melt-$H_2O$-$CO_2$ solution model written in Visual Basic for Excel. Computers & Geosciences, 28(5), 597-604.

Papale, P., Moretti, R., and Barbato, D. (2006) The compositional dependence of the saturation surface of $H_2O$ + $CO_2$ fluids in silicate melts. Chemical Geology, 229(1-3), 78-95.

Peppard, B.T., Steele, I.M., Davis, A.M., Wallace, P.J., and Anderson, A.T. (2001) Zoned quartz phenocrysts from the rhyolitic Bishop Tuff. American Mineralogist, 86(9), 1034-1052.

Putirka, K.D. (2005) Igneous thermometers and barometers based on plagioclase + liquid equilibria: Tests of some existing models and new calibrations. American Mineralogist, 90(2-3), 336-346.

-. (2008) Thermometers and Barometers for Volcanic Systems. Reviews in Mineralogy and Geochemistry, 69(1), 61-120.

Rapien, M.H. (1998) Geochemical Evolution at White Island, New Zealand. department of Geosciences, Master's, p. 59. Virginia Tech, Blacksburg, VA.

Rapien, M.H., Bodnar, R.J., Simmons, S.F., Szabo, C., and Sutton, S.R. (2003) The embryonic porphyry copper system at White Island, New Zealand. Society of Economic Geologists, Special Publication 10, 2003, p. 41–59, 10, 41-59.

1240 Roberge, J., Wallace, P.J., and Kent, A.J.R. (2013) Magmatic processes in the Bishop
1241 Tuff rhyolitic magma based on trace elements in melt inclusions and pumice
1242 matrix glass. Contributions to Mineralogy and Petrology, 165(2), 237-257.
1243 Roedder, E. (1979) Origin and significance of magmatic inclusions. Bulletin de
1244 Mineralogie, 102(5-6, Mineraux et Minerais), 487-510.
1245 Rose, W.I., Chuan, R.L., Giggenbach, W.F., and Symonds, R.B. (1986) Rates of sulphur
1246 dioxide and particle emissions from White Island volcano, New Zealand, and an
1247 estimate of the total flux of major gaseous species. Bulletin of Volcanology,
1248 48(4), 181-188.
1249 Schiffbauer, J.D., and Xiao, S. (2009) Novel application of focused ion beam electron
1250 microscopy (FIB-EM) in preparation and analysis of microfossil ultrastructures:
1251 A new view of complexity in early Eukaryotic organisms. PALAIOS, 24(9), 616-
1252 626.
1253 Schiffbauer, J.D., and Xiao, S. (2011) Paleobiological Applications of Focused Ion Beam
1254 Electron Microscopy (FIB-EM): An Ultrastructural Approach to the (Micro)Fossil
1255 Record
1256 Quantifying the Evolution of Early Life. In M. Laflamme, J.D. Schiffbauer, and S.Q.
1257 Dornbos, Eds, 36, p. 321-354. Springer Netherlands.
1258 Severs, M.J., Azbej, T., Thomas, J.B., Mandeville, C.W., and Bodnar, R.J. (2007)
1259 Experimental determination of H2O loss from melt inclusions during laboratory
1260 heating: Evidence from Raman spectroscopy. Chemical Geology, 237(3–4), 358-
1261 371.
1262 Severs, M.J., Beard, J.S., Fedele, L., Hanchar, J.M., Mutchler, S.R., and Bodnar, R.J.
1263 (2009) Partitioning behavior of trace elements between dacitic melt and
1264 plagioclase, orthopyroxene, and clinopyroxene based on laser ablation ICPMS
1265 analysis of silicate melt inclusions. Geochimica Et Cosmochimica Acta, 73(7),
1266 2123-2141.
1267 Sherburn, S., Scott, B.J., Nishi, Y., and Sugihara, M. (1998) Seismicity at White Island
1268 volcano, New Zealand: a revised classification and inferences about source
1269 mechanism. Journal of Volcanology and Geothermal Research, 83(3–4), 287-312.
1270 Sisson, T.W., and Bronto, S. (1998) Evidence for pressure-release melting beneath
1271 magmatic arcs from basalt at Galunggung, Indonesia. Nature, 391(6670), 883-
1272 886.
1273 Sisson, T.W., and Layne, G.D. (1993) H2O in basalt and basaltic andesite glass
1274 inclusions from four subduction-related volcanoes. Earth and Planetary Science
1275 Letters, 117(3–4), 619-635.
1276 Sobolev, A.V., and Kostyuk, V.P. (1976) Magmatic crystallization based on study of
1277 melt inclusions. Fluid inclusion research, 9, 182-253.
1278 Sparks, R.S.J. (1978) The dynamics of bubble formation and growth in magmas: A
1279 review and analysis. Journal of Volcanology and Geothermal Research, 3(1–2), 1-
1280 37.
1281 Spilliaert, N., Allard, P., Métrich, N., and Sobolev, A.V. (2006) Melt inclusion record of
1282 the conditions of ascent, degassing, and extrusion of volatile-rich alkali basalt
1283 during the powerful 2002 flank eruption of Mount Etna (Italy). Journal of
1284 Geophysical Research: Solid Earth, 111(B4), B04203.

Steele-MacInnis, M.J., Esposito, R., and Bodnar, R.J. (2011) Thermodynamic model for the effect of post-entrapment crystallization on the $H_2O$-$CO_2$ systematics of volatile saturated silicate melt inclusions. . Journal of Petrology, 52(12), 2461-2482.

Tedesco, D., and Toutain, J.-P. (1991) Chemistry and emission rate of volatiles from White Island Volcano (New Zealand). Geophysical Research Letters, 18(1), 113-116.

Tomiya, A., and Takahashi, E. (2005) Evolution of the magma chamber beneath Usu Volcano since 1663; a natural laboratory for observing changing phenocryst compositions and textures. Journal of Petrology, 46(12), 2395-2426.

Vigouroux, N., Wallace, P.J., and Kent, A.J.R. (2008) Volatiles in High-K Magmas from the Western Trans-Mexican Volcanic Belt: Evidence for Fluid Fluxing and Extreme Enrichment of the Mantle Wedge by Subduction Processes. Journal of Petrology, 49(9), 1589-1618.

Wade, J.A., Plank, T., Melson, W.G., Soto, G.J., and Hauri, E.H. (2006) The volatile content of magmas from Arenal Volcano, Costa Rica. Journal of volcanology and geothermal research, 157(1-3), 94-120.

Wallace, P.J. (2005) Volatiles in subduction zone magmas: concentrations and fluxes based on melt inclusion and volcanic gas data. Journal of Volcanology and Geothermal Research, 140(1–3), 217-240.

Wallace, P.J., Anderson, A.T., and Davis, A.M. (1999) Gradients in H2O, CO2, and exsolved gas in a large-volume silicic magma system: Interpreting the record preserved in melt inclusions from the Bishop Tuff. Journal of Geophysical Research: Solid Earth, 104(B9), 20097-20122.

Wardell, L.J., Kyle, P.R., Dunbar, N., and Christenson, B. (2001) White Island Volcano, New Zealand; carbon dioxide and sulfur dioxide emission rates and melt inclusion studies. In D. Bergfeld, F. Goff, and P. Allard, Eds. Chemical Geology, 177, p. 187-200. Elsevier, Amsterdam.

Welsch, B., Faure, F., Famin, V., Baronnet, A., and Bachèlery, P. (2013) Dendritic Crystallization: A Single Process for all the Textures of Olivine in Basalts? Journal of Petrology, 54(3), 539-574.

Zhang, Y., and Ni, H. (2010) Diffusion of H, C, and O Components in Silicate Melts. Reviews in Mineralogy and Geochemistry, 72(1), 171-225.

## FIGURE CAPTIONS

Fig. 1. Major element compositions of MI from recent eruptions (1977, 1986, 1988, and 1989) at White Island, New Zealand, compared to bulk rock compositions. MI data are from the literature (Rapien, 1998; Severs et al., 2009; Wardell et al., 2001). The bulk rock

data are from Graham and Cole (1991) and Cole et al. (2000). a, c, e) $FeO_{tot}$ (a), MgO (c) and CaO (e) vs. $SiO_2$ for MI classified by the eruption year. b, d, f) $FeO_{tot}$ (b), MgO (d) and CaO (f) vs. $SiO_2$ for MI from the 1988 eruption classified according to host phase. Data for in Figs 1b, d and f are from Severs et al. (2009). Filled symbols refer to MI analyzed by LA-ICPMS, while open symbols refer to MI analyzed by EMP. Note the small variation in major element concentrations of the MI, especially for the 1986 eruption. Also, note that the $FeO_{tot}$ content of MI is consistent with the $SiO_2$ vs. $FeO_{tot}$ trend defined by the bulk rock, suggesting that the MI have not experienced Fe loss or gain. MI compositions extend from the bulk rock trend towards more evolved (dacitic) composition. MI studied by Wardell et al. (2001) (see the arrows in panels a, c, e) show slightly less evolved compositions compared to MI reported by Rapien (1998) and Severs et al. (2009).

Fig. 2. Photomicrograph of MIA hosted in olivine (RESC5-O21) from the Solchiaro eruption (left) and $Al_2O_3$ vs. $CO_2$ systematics of MI (right) (modified from Esposito et al., 2011). a) BSE image showing slight normal zonation and a forsterite-rich rim. The white background represents the indium mount, and the dashed red line represents the olivine boundary (partially beneath the surface and covered by indium). The solid red lines identify a growth zone containing the MIA and spinel inclusions parallel to the olivine border. b) $Al_2O_3$ vs. $CO_2$ diagram of MI from sample RESC5 (Esposito et al., 2011). Note the consistent trend defined by bubble-free MI.

Fig. 3. Photomicrograph of MIA hosted in plagioclase from the White Island volcano in New Zealand, taken in reflected light, showing laser-drilled holes around exposed MI. MIA are marked by the red dashed lines and are parallel to the boundaries of the euhedral phenocryst. Various types of MI and MIA (based on the phases in the MI) can be observed in this plagioclase phenocryst (see text for more details).

Fig. 4. Clinopyroxene phenocryst from White Island scoriae showing characteristic growth zones defined by the entrapment of inclusions (MI, mixed MI and solid inclusions). The white dashed lines highlight a melt inclusion assemblage (MIA).

Fig. 5. FIB-EM image of a MI hosted in plagioclase (plg) from White Island. The sample surface is titled by 52° from horizontal. The dashed line indicates the MI/host boundary. A laser ablation pit (laser shot) used to help locate the MI during SIMS analysis is visible on the left side of the photo. Note the regularity of the MI/host interface in the vertical section.

Fig. 6. FIB-EM image of a MI hosted in olivine from the Solchiaro eruption, Procida Island, Italy. Note the irregularity of the MI/host bottom interface (dashed white line). "Oli" represents the olivine host.

Fig. 7. Box-and-Whisker plots for $H_2O$, F, and Cl contents of MIA hosted in clinopyroxene, orthopyroxene and plagioclase from White Island. The box limits are the $25^{th}$ and $75^{th}$ percentiles, and the upper and lower limits of the bars represent the

1370 maximum and minimum concentrations. Note the consistency of concentrations in MI
1371 within a single MIA. Black squares are data point (MI) relative to single MIA and
1372 diamonds represent the means of each MIA.
1373
1374 Fig. 8. Box-and-Whisker plots for $CO_2$ and S contents of zonal and azonal MIA hosted in
1375 clinopyroxene, orthopyroxene and plagioclase from White Island. The box limits are the
1376 $25^{th}$ and $75^{th}$ percentiles, and the upper and lower limits of the bars represent the
1377 maximum and minimum concentrations. Note the significant scatter in $CO_2$ contents
1378 within a single MIA for about half of the all MIA analyzed. Also, note that S
1379 concentrations are consistent in MIA hosted in plagioclase, and that the concentration of
1380 $CO_2$ is <200 ppm for MIA that show little variability. In addition, it is important to note
1381 that only two zonal MIA show inconsistent results for S contents. Symbols are as in Fig.
1382 7.
1383
1384 Fig. 9. $H_2O$-$CO_2$ systematics of three different zonal MIA. a) degassing paths fit to data
1385 from MI of MIA-08 hosted in plagioclase; b) degassing paths fit to data from MI of MIA-
1386 13 hosted in plagioclase; c) degassing paths fit to data from MI from MIA-16 hosted in
1387 clinopyroxene. The green arrow indicates a closed-system degassing path and the blue-
1388 dashed arrows indicates an open-system degassing path. The degassing paths were
1389 calculated using the VolatileCalc software by Newman and Lowenstern (2002) for a
1390 basaltic composition at 1250ºC, based on heating experiments on MI reported by Rapien
1391 et al. (2003). The starting volatile compositions are based on the most $CO_2$-rich MI

obtained from each MIA considered. The closed-system degassing path was calculated assuming <10% of gas coexisting with the melt.

Fig. 10. Box-and-Whisker plots for (a) $H_2O$, (b) F, (c) Cl, (d) $CO_2$ and (e) S concentrations of MIA hosted in olivine and clinopyroxene from the Solchiaro eruption, Island of Procida, Italy. The box limits are the $25^{th}$ and $75^{th}$ percentiles, and the upper and lower limits of the bars represent the maximum and minimum concentrations. Note that the $CO_2$ variability of MIA from Solchiaro (panel d) is less than that of the White Island MIA. Also, it is important to note that there is no correlation between the type of MIA (azonal and zonal) and the degree of $CO_2$ variability. Symbols are as in Fig. 7.

Fig. 11. Box-and-Whisker plots for $CO_2$ concentrations of single MI. Data include results from Esposito et al. (2011). The box limits are the $25^{th}$ and $75^{th}$ percentiles, and the upper and lower limits of the bars represent the maximum and minimum concentrations. a) $CO_2$ variability of all MI that were measured multiple times; b) enlargement of the low $CO_2$ portion of the diagram to better illustrate the $CO_2$-poor MI. Note the y-axes are in logarithmic scale. Symbols are as in Fig. 7.

Fig. 12. $CO_2$ depth profiles of exposed and unexposed MI from White Island and Solchiaro. a) $CO_2$ depth profiles for MI hosted in plagioclase from White Island. Note the erratic $CO_2$ behavior in the shallowest part of the MI. All the profiles refer to exposed MI with the exception of the blue profile that refers to an unexposed MI (Dec 7_5 MI). The unexposed MI is the same one shown in Fig.13. The boundary between the melt and the

host is at ~ 5000 sec (see Fig.13) and, thus, is not shown in this figure; b) $CO_2$ depth profiles for MI hosted in mafic phenocrysts. The purple, green, and orange profiles refer to MI from Solchiaro and are hosted in olivine, while the blue and the black profiles refer to MI from White Island and hosted in orthopyroxene and clinopyroxene respectively. The shallowest parts of the profiles do not show the same erratic behavior for $CO_2$ exhibited by MI hosted in plagioclase (panel a). The green and the blue profiles are from unexposed MI hosted in olivine and in clinopyroxene, respectively. The orange, blue, and black lines go to essentially zero and are not resolvable on this figure. The MI/host interface is at around 7000 sec for the MI hosted in olivine and around 4000 sec for the MI hosted in clinopyroxene. The other three profiles refer to MI exposed at the surface; c) $CO_2$ depth profiles for glass standards and blanks used to determine the calibration curves. Note that $CO_2$ concentrations do not show anomalous behavior in the glass standards. The solid vertical lines indicate the duration of the pre-sputtering and the analysis that was used most commonly for our MI analyses. Thus, the somewhat erratic behavior observed in the first few hundred seconds here would normally have been part of the pre-sputtering to remove surface effects and would not have been included in the quantification of $CO_2$ in the MI.

Fig. 13. a) $CO_2$ depth profile for an unexposed MI hosted in plagioclase analyzed by SIMS. Note the anomalous behavior of the $CO_2$ profile, which shows two enrichments near the MI/host interface. A profilometer was used to measure the depth of the SIMS crater shown on the right ordinate. The black dashed line represents the inferred position of the host/MI interface. Note that the MI/host interface cannot be a definite line in the

profile diagram; rather, there is a transition zone where both the glass of the MI and the host are analyzed together. The pink background represents the part of the profile interpreted to represent material contaminated with C. The yellow background represents the plagioclase host. b) FIB-EM image of the analyzed MI hosted in plagioclase. The dashed red lines represent the open pit on the surface of the plagioclase and the host/MI interface. Note that the host/MI interface is sub-parallel to the sample polished-section.

Fig. 14. Box-and-Whisker plots for Relative Standard Deviation (RSD) of MIA hosted in clinopyroxene, orthopyroxene, plagioclase, and olivine from White Island and Solchiaro. The box limits are the $25^{th}$ and $75^{th}$ percentiles, and the upper and lower limits of the bars represent the maximum and minimum concentrations. Note the wider RSD variability of $CO_2$ relative to that of the other volatiles considered in this study.

**Deposit Item captions**

Deposit Item-01-01. Calibration curves for $CO_2$ analyzed by SIMS at Virginia Tech. Known standard $CO_2$ concentrations are plotted versus $^{12}C/^{30}Si$ isotope ratios measured by SIMS. The ratio is expressed as the ion count per second of $^{12}C$ divided by the ion counts per second of $^{30}Si$. In the diagrams we have reported the linear regressions forced to go through the origin. Data used for the calibration are reported in Appendix Table 1. Panels a, b, c, d, e, and f show calibration curves for each working session at Virginia Tech in May 2008, December 2008, March 2010, December 2010, October 2011, and

March 2012, respectively. Note that $CO_2$ calibration curves calculated for this study are consistent with those reported by Helo et al. (2011).

Deposit Item-01-02. Calibration curves for $H_2O$ analyzed by SIMS at Virginia Tech. Known standard $H_2O$ concentrations are plotted versus $^{16}O^{1}H/^{30}Si$ isotope ratios measured by the SIMS. The ratio is expressed as the ion count per second of $^{16}O^{1}H$ divided by the ion counts per second of $^{30}Si$. In the diagrams we have reported the linear regressions forced to go through the origin. Data used for the calibration are reported in Appendix Table 1. Panels a, b, c, d, and e show calibration curves representative of each working session at Virginia Tech in May 2008, December 2008, March 2010, December 2010, October 2011, and March 2012, respectively. Note that $H_2O$ calibration curves calculated for this study are consistent with those reported by Helo et al. (2011).

Deposit Item-01-03. Calibration curves for F analyzed by SIMS at Virginia Tech. Known standard F concentrations are plotted versus $^{19}F/^{30}Si$ isotope ratios measured by SIMS. The ratio is expressed as the ion count per second of $^{19}F$ divided by the ion counts per second of $^{30}Si$. In the diagrams we have reported the linear regressions forced to go through the origin. Data used for the calibration are reported in Appendix Table 1. Panels a, b, c, d, and e show calibration curves representative of each working session at Virginia Tech in May 2008, December 2008, March 2010, December 2010, and October 2011respectively. Note that the F calibration curves calculated for this study are consistent with those reported by Helo et al. (2011).

Deposit Item-01-04. Calibration curves of S analyzed by SIMS at Virginia Tech. Known standard S concentrations are plotted versus $^{32}S/^{30}Si$ isotope ratios measured by SIMS. The ratio is expressed as the ion count per second of $^{32}S$ divided by the ion counts per second of $^{30}Si$. In the diagrams we have reported the linear regressions forced to go through the origin. Data used for the calibration are reported in Appendix Table 1. Panels a, b, c, d, and e show calibration curves representative of each working session at Virginia Tech in May 2008, December 2008, March 2010, December 2010, October 2011, and March 2012, respectively. Note that the S calibration curves calculated for this study are consistent with those reported by Helo et al. (2011).

Deposit Item-01-05. Calibration curves for Cl analyzed by SIMS at Virginia Tech. Known standard Cl concentrations are plotted versus $^{35}Cl/^{30}Si$ isotope ratios measured by SIMS. The ratio is expressed as the ion count per second of $^{35}Cl$ divided by the ion counts per second of $^{30}Si$. In the diagrams we have reported the linear regressions forced to go through the origin. Data used for the calibration are reported in Appendix Table 1. Panels a, b, c, d, and e show calibration curves representative of each working session at Virginia Tech in May 2008, December 2008, March 2010, December 2010, October 2011, and March 2012, respectively. Note that the Cl calibration curves calculated for this study are consistent with those reported by Helo et al. (2011).

Deposit Item-01-06. Calibration curves for $CO_2$, $H_2O$, and F analyzed by SIMS at WHOI. Known concentrations of standard glasses are plotted versus $^{12}C/^{30}Si$, $^{16}O^{1}H/^{30}Si$, and $^{19}F/^{30}Si$ isotope ratios measured using SIMS. The ratio is expressed as the ion count per

second of $^{12}C$, $^{16}O^{1}H$, $^{19}F$ divided by the ion counts per second of $^{30}Si$. In the diagrams we have reported the linear regressions forced to go through the origin. Data used for the calibration are reported in Appendix Table 1. Panels a, c, e, show calibration curves for February 2011 working session at WHOI. Panels b, d, f show calibration curves for January 2013 working session at WHOI. Note that $CO_2$, $H_2O$, and F calibration curves calculated for this study are consistent with those reported by Helo et al. (2011).

Deposit Item-01-07. Calibration curves for S and Cl analyzed by SIMS at WHOI. Known concentrations of standard glasses are plotted versus $^{32}S/^{30}Si$ and $^{35}F/^{30}Si$ isotope ratios measured using SIMS. The ratio is expressed as the ion count per second of $^{32}S$ and $^{35}F$ divided by the ion counts per second of $^{30}Si$. In the diagrams we have reported the linear regressions forced to go through the origin. Data used for the calibration are reported in Appendix Table 1. Panels a and c show calibration curves for February 2011 working session at WHOI. Panels b and d show calibration curves for January 2013 working session at WHOI. Note that S and Cl calibration curves calculated for this study are consistent with those reported by Helo et al. (2011).

Deposit Item-01-08. $CO_2$ and $H_2O$ calibration curves of January 2013 sessions at WHOI showing the $CO_2$-rich and the $H_2O$-rich standard glasses included for the calibration of this session. It is important to note that the slopes of calibration curves for the January 2013 session are consistent with the slopes of the previous working sessions both at Virginia Tech and WHOI.

Deposit Item-02. Photomicrograph of a "pseudosecondary MIA" hosted in pyroxene from White Island observed in transmitted light. Notice the more elongated shape of the MI in this MIA relative to those shown in Figures 3 and 4.

Deposit Item-03. Variability in $H_2O$ contents observed in different analytical sessions. Note that concentrations from the October 2011 session are slightly higher, and those from March 2010 are slightly lower, than those from the other working sessions. It is important to note that the same MI (RESC5-O27-MF from Solchiaro sample) was measured in different working sessions. The concentration variability likely reflects slight differences in the calibration curves determined for each working session (see Supplementary Material for more details).

Deposit Item-04. $CO_2$-depth profile of one MI (860210-MI-8) from the 1986 eruption at White Island measured at WHOI during the January 2013 session (Table 5). The profile is the compilation of two analyses done on the same spot inside the MI. As reported in the text, it is important to note that the concentration varies from 608 ppm (the shallowest glass analyzed) to 282 ppm (the deepest glass analyzed). The data used for this plot are reported in Appendix Table 1.

This is a preprint, the final version is subject to change, of the American Mineralogist (MSA)
Cite as Authors (Year) Title. American Mineralogist, in press.
(DOI will not work until issue is live.) DOI: http://dx.doi.org/10.2138/am.2014.4574 

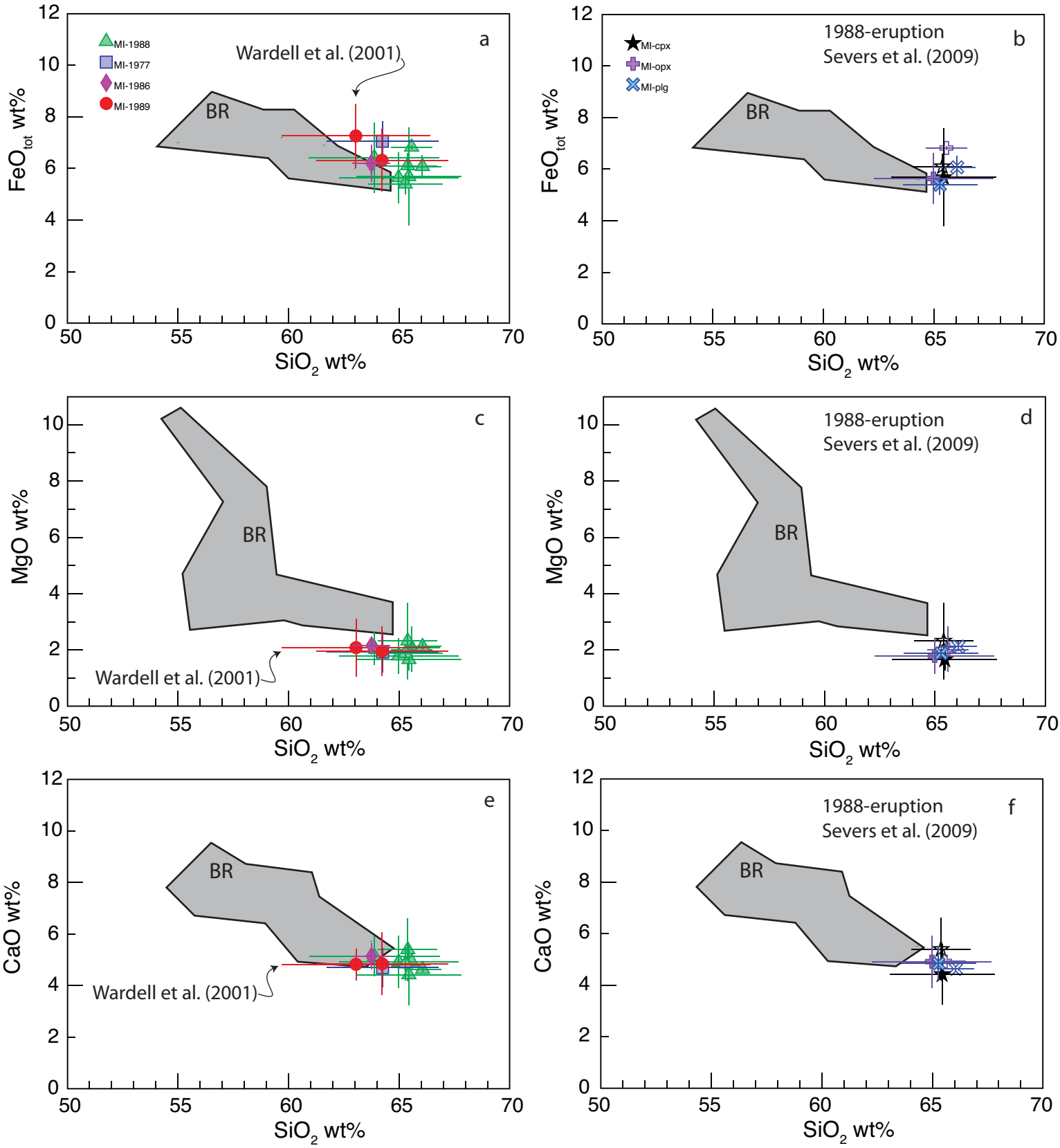


Fig. 1

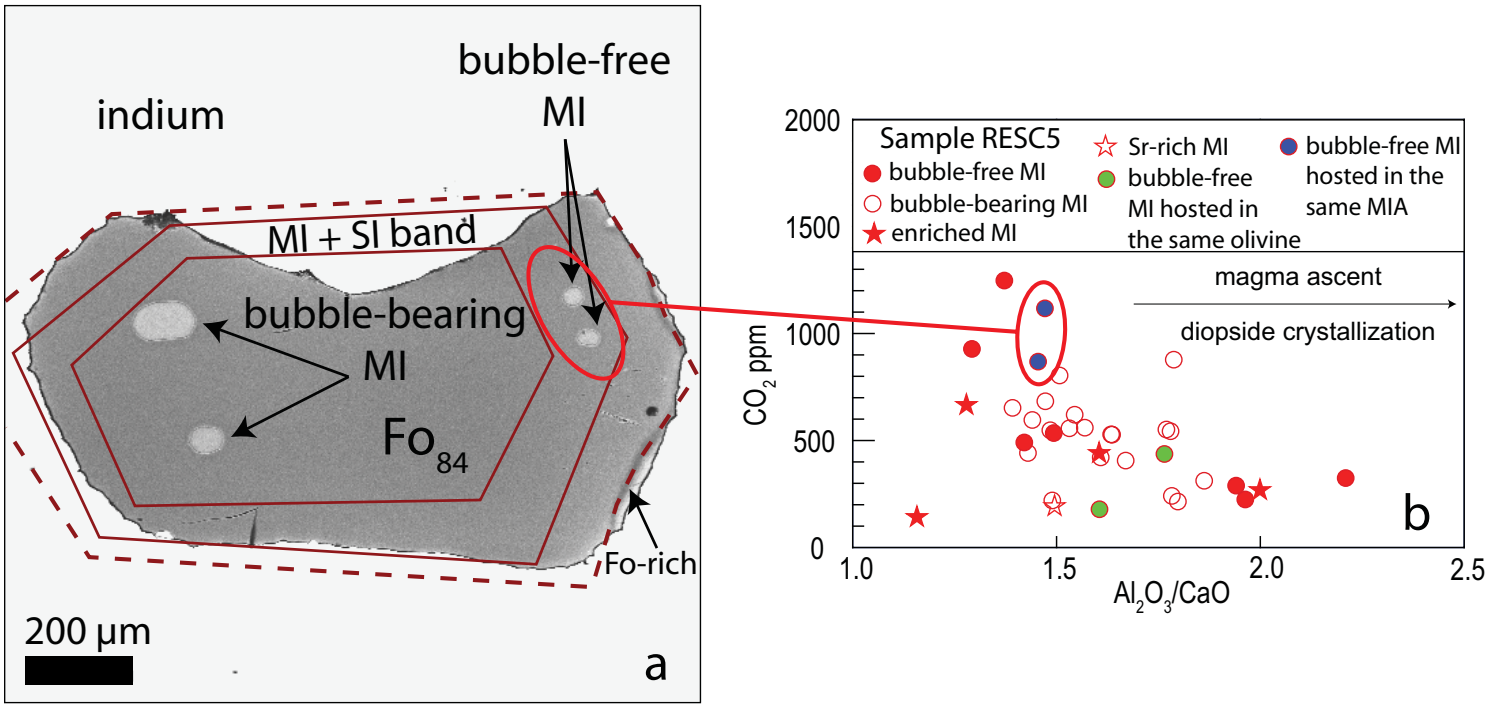
indium
bubble-free MI
MI + SI band
bubble-bearing MI
Fo84
Fo-rich
200 µm
a
Sample RESC5
bubble-free MI
bubble-bearing MI
enriched MI
Sr-rich MI
bubble-free MI hosted in the same olivine
bubble-free MI hosted in the same MIA
magma ascent
diopside crystallization
CO2 ppm
Al2O3/CaO
2000
1500
1000
500
0
1.0
1.5
2.0
2.5
b

Fig. 2

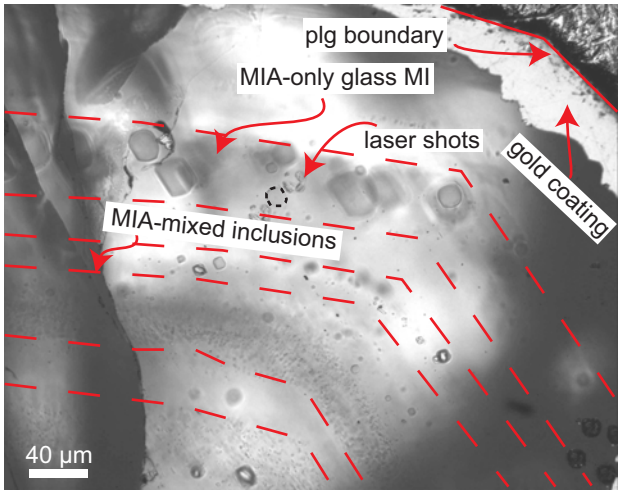
plg boundary
MIA-only glass MI
laser shots
gold coating
MIA-mixed inclusions
40 µm

Fig. 3

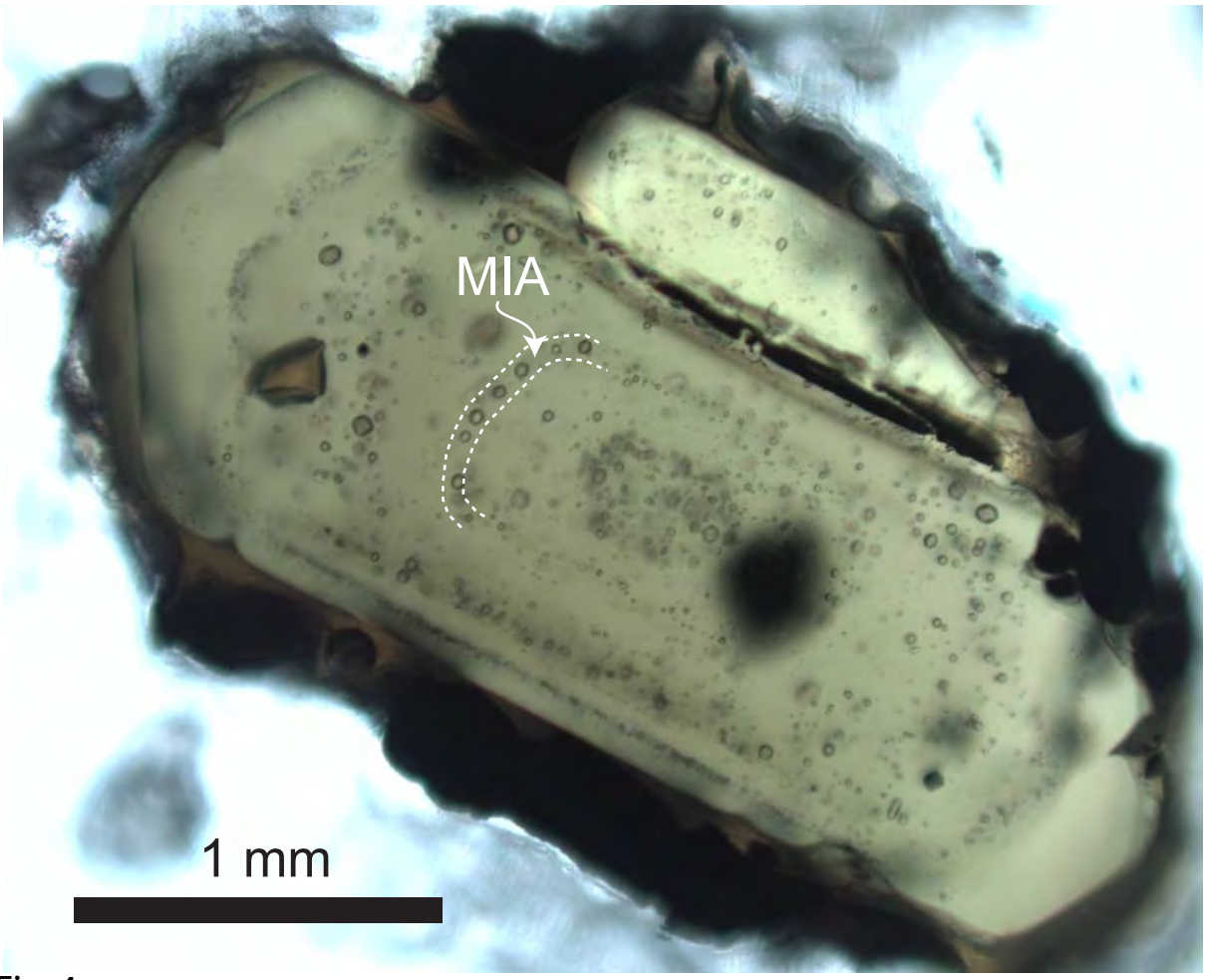


Fig. 4

This is a preprint, the final version is subject to change, of the American Mineralogist (MSA)
Cite as Authors (Year) Title. American Mineralogist, in press.
(DOI will not work until issue is live.) DOI: http://dx.doi.org/10.2138/am.2014.4574 

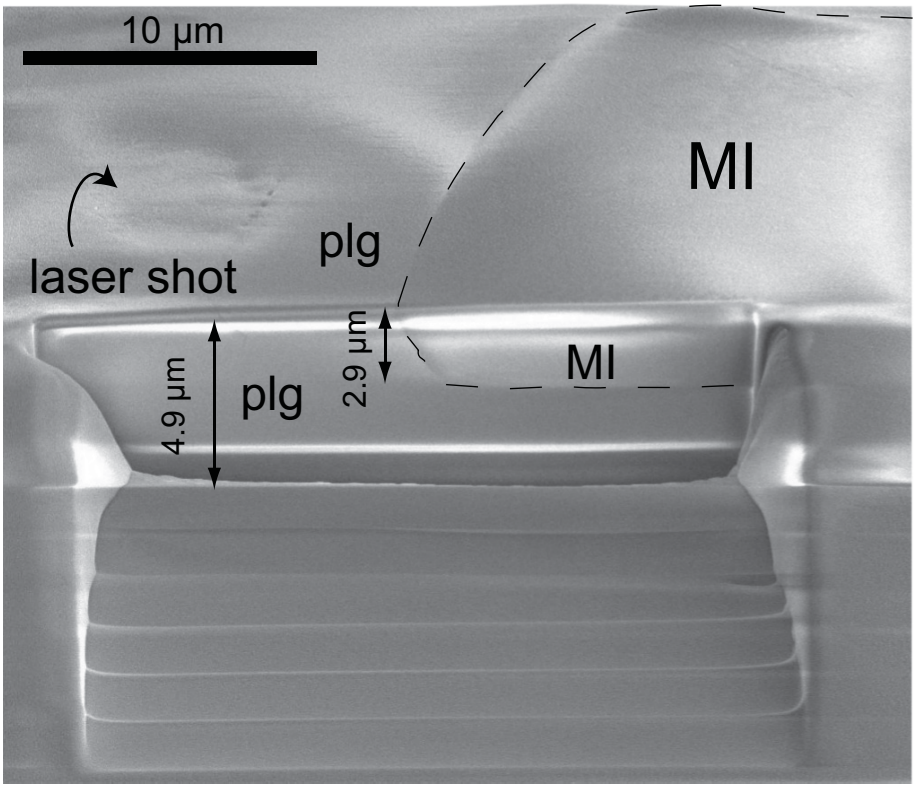


Fig. 5

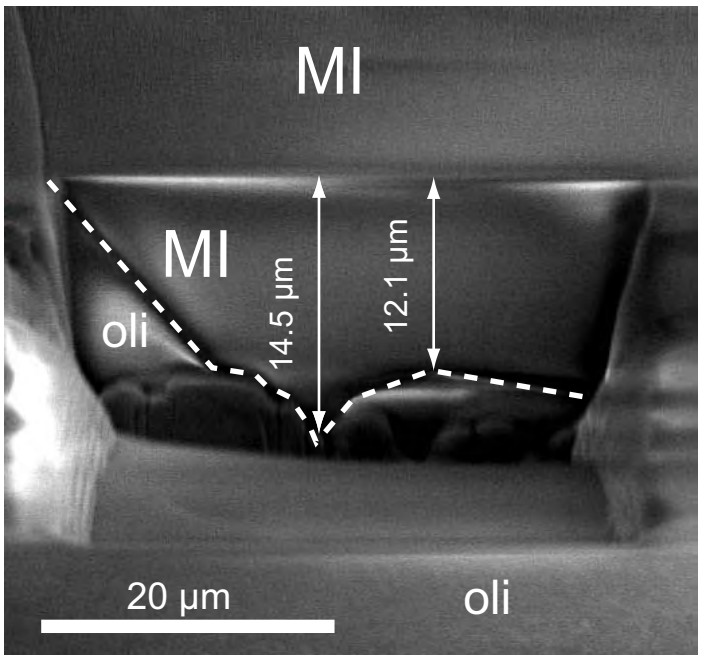


Fig. 6

This is a preprint, the final version is subject to change, of the American Mineralogist (MSA)
Cite as Authors (Year) Title. American Mineralogist, in press.
(DOI will not work until issue is live.) DOI: http://dx.doi.org/10.2138/am.2014.4574 

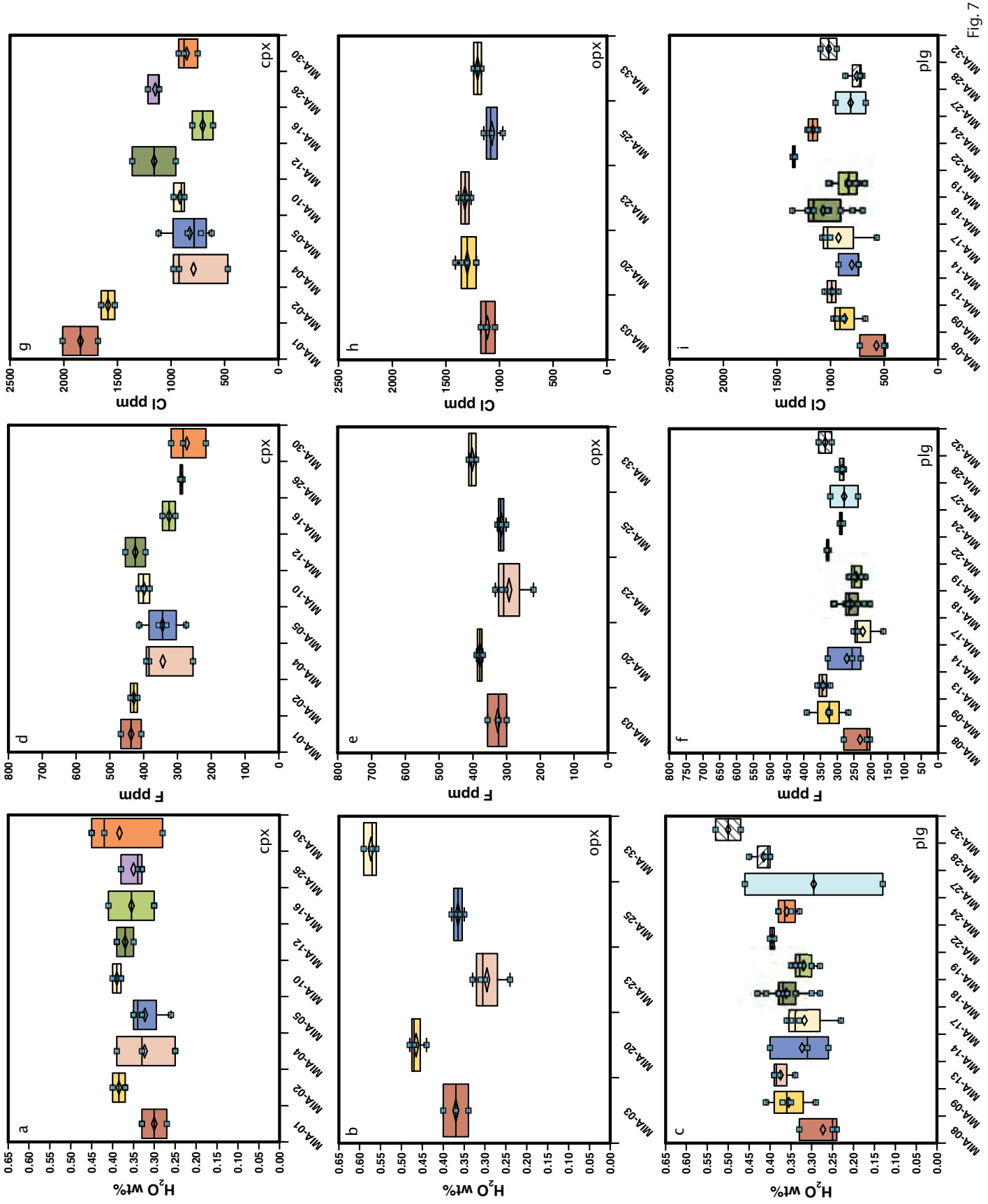


Fig. 7

This is a preprint, the final version is subject to change, of the American Mineralogist (MSA)
Cite as Authors (Year) Title. American Mineralogist, in press.
(DOI will not work until issue is live.) DOI: http://dx.doi.org/10.2138/am.2014.4574 

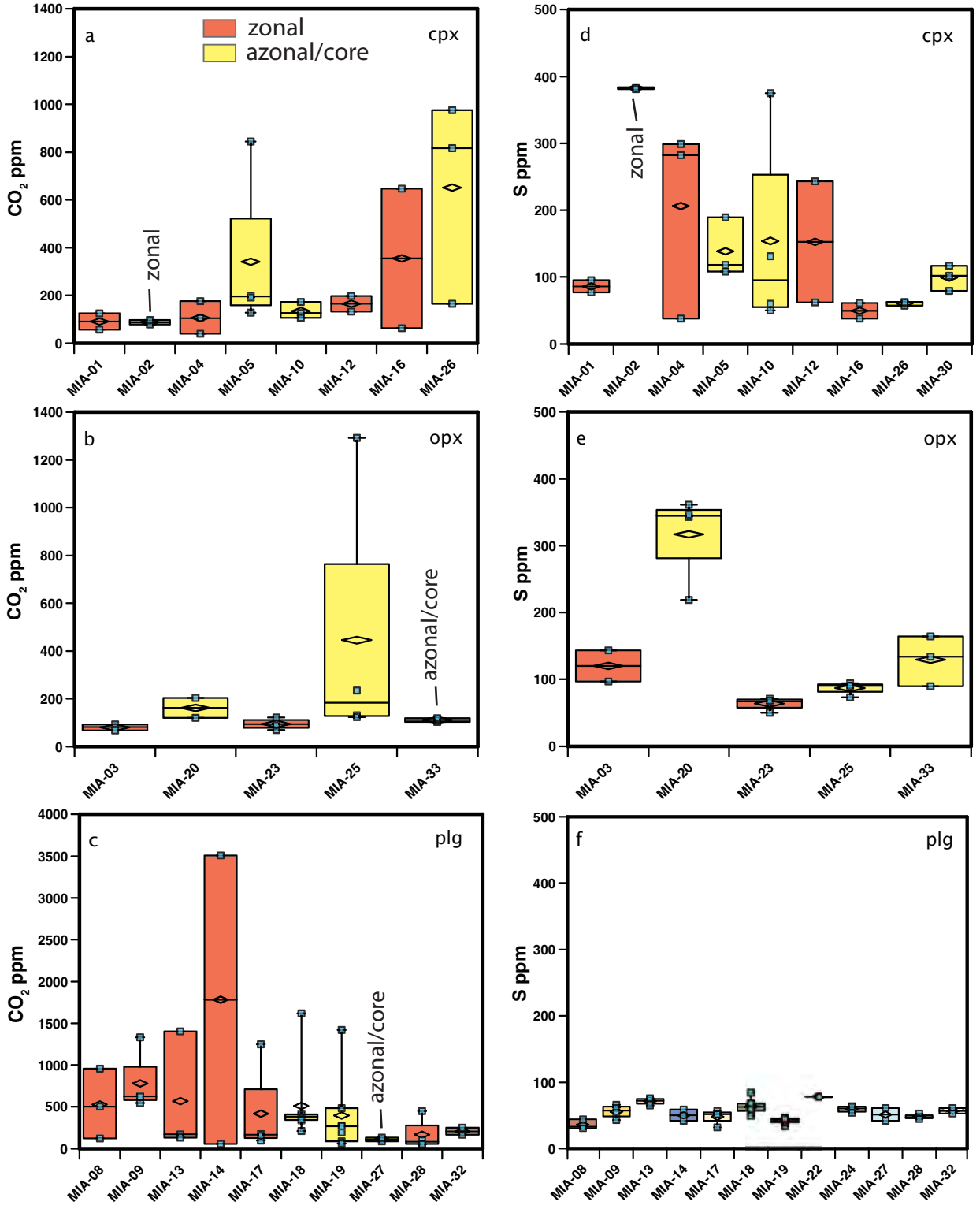


Fig. 8

This is a preprint, the final version is subject to change, of the American Mineralogist (MSA)
Cite as Authors (Year) Title. American Mineralogist, in press.
(DOI will not work until issue is live.) DOI: http://dx.doi.org/10.2138/am.2014.4574


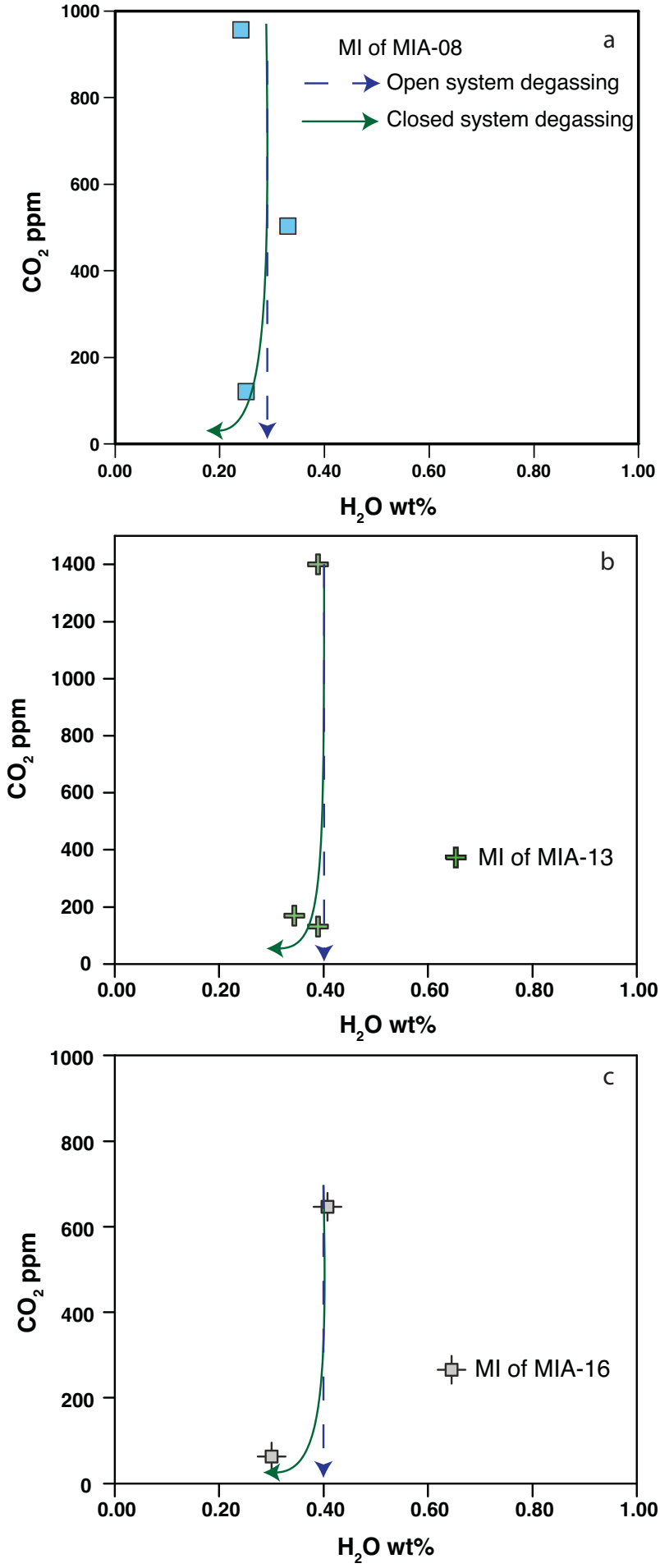


Fig. 9

This is a preprint, the final version is subject to change, of the American Mineralogist (MSA)
Cite as Authors (Year) Title. American Mineralogist, in press.
(DOI will not work until issue is live.) DOI: http://dx.doi.org/10.2138/am.2014.4574 

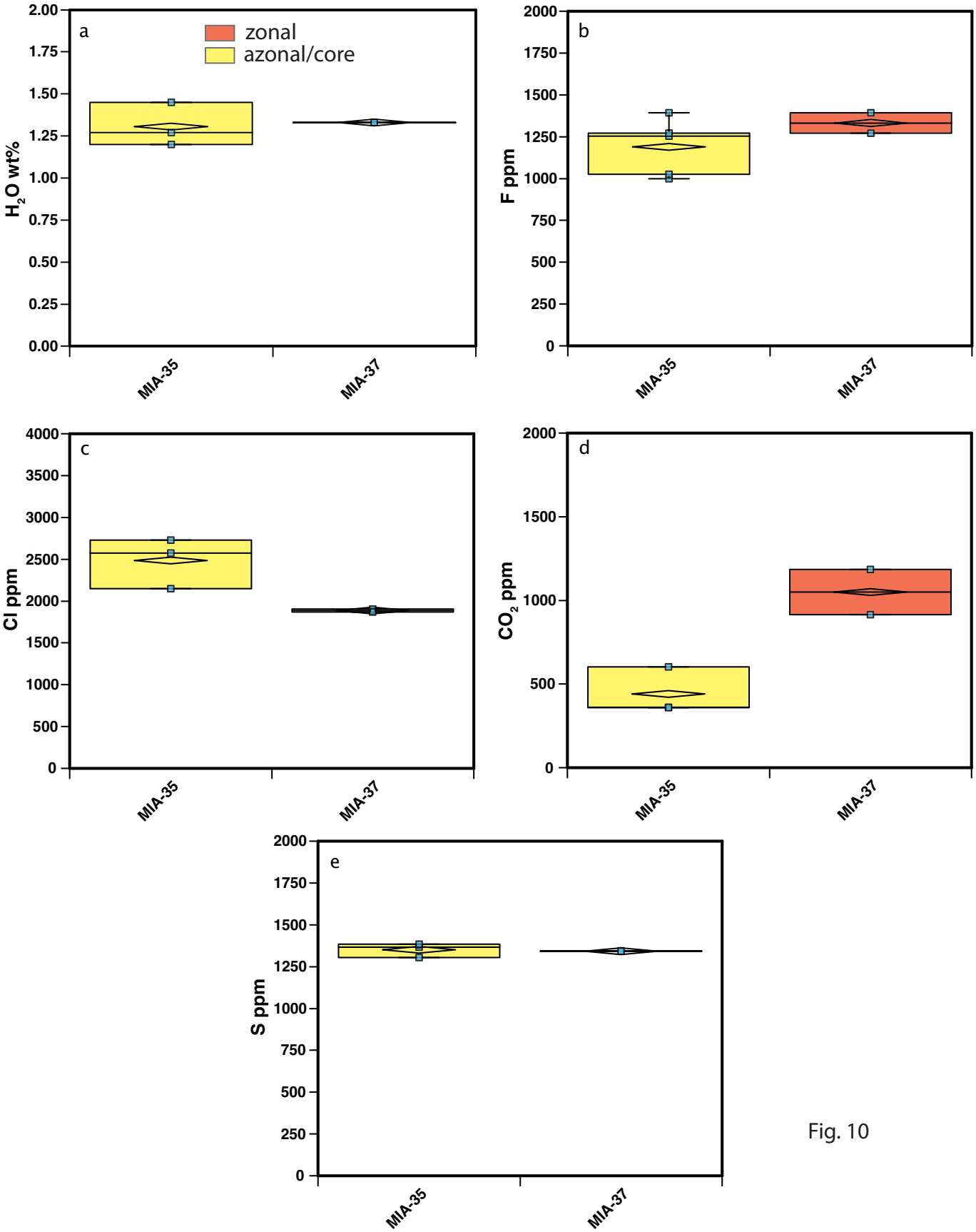


Fig. 10

This is a preprint, the final version is subject to change, of the American Mineralogist (MSA)
Cite as Authors (Year) Title. American Mineralogist, in press.
(DOI will not work until issue is live.) DOI: http://dx.doi.org/10.2138/am.2014.4574 

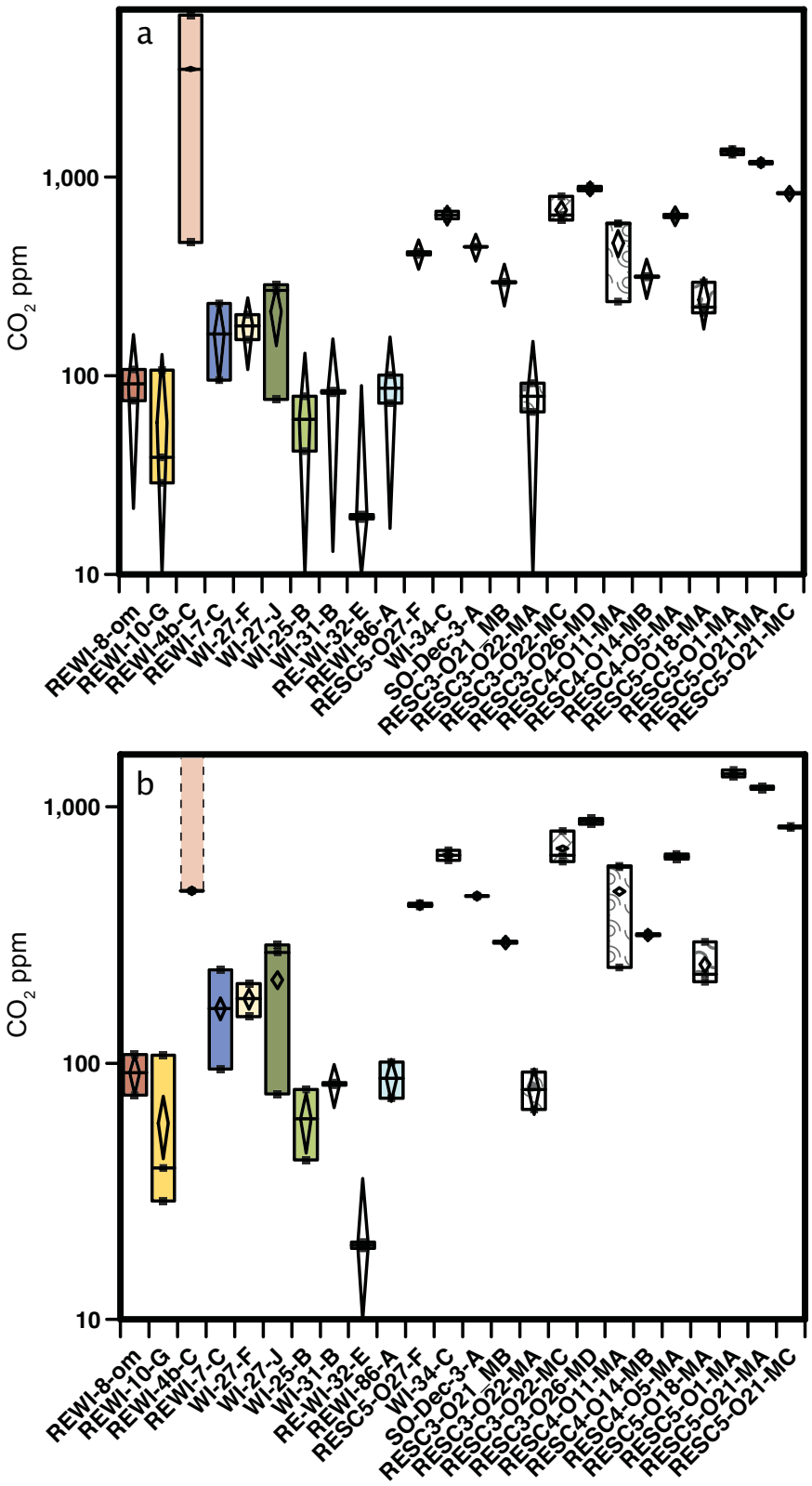


Fig. 11

This is a preprint, the final version is subject to change, of the American Mineralogist (MSA)
Cite as Authors (Year) Title. American Mineralogist, in press.
(DOI will not work until issue is live.) DOI: http://dx.doi.org/10.2138/am.2014.4574


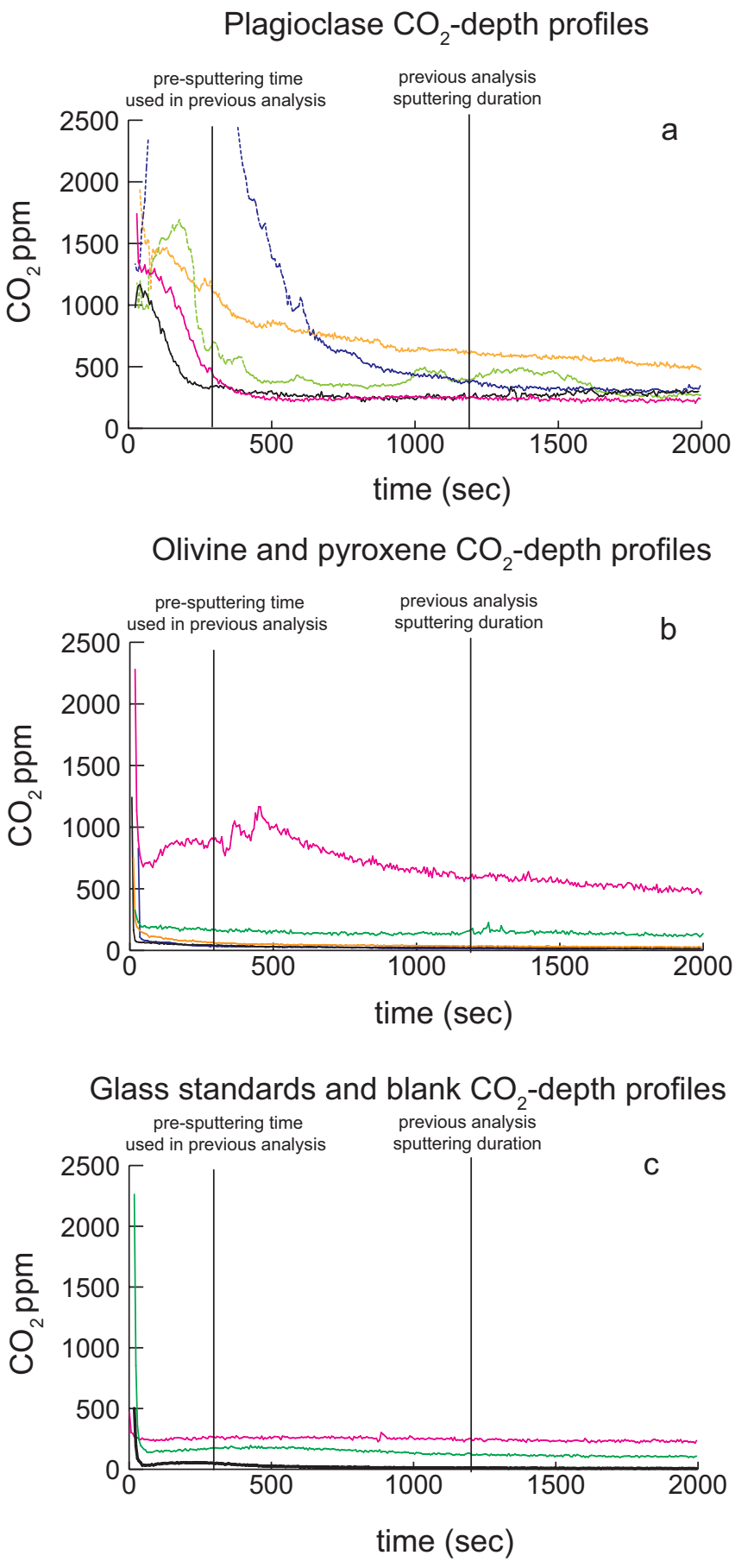


Fig. 12

This is a preprint, the final version is subject to change, of the American Mineralogist (MSA)
Cite as Authors (Year) Title. American Mineralogist, in press.
(DOI will not work until issue is live.) DOI: http://dx.doi.org/10.2138/am.2014.4574 

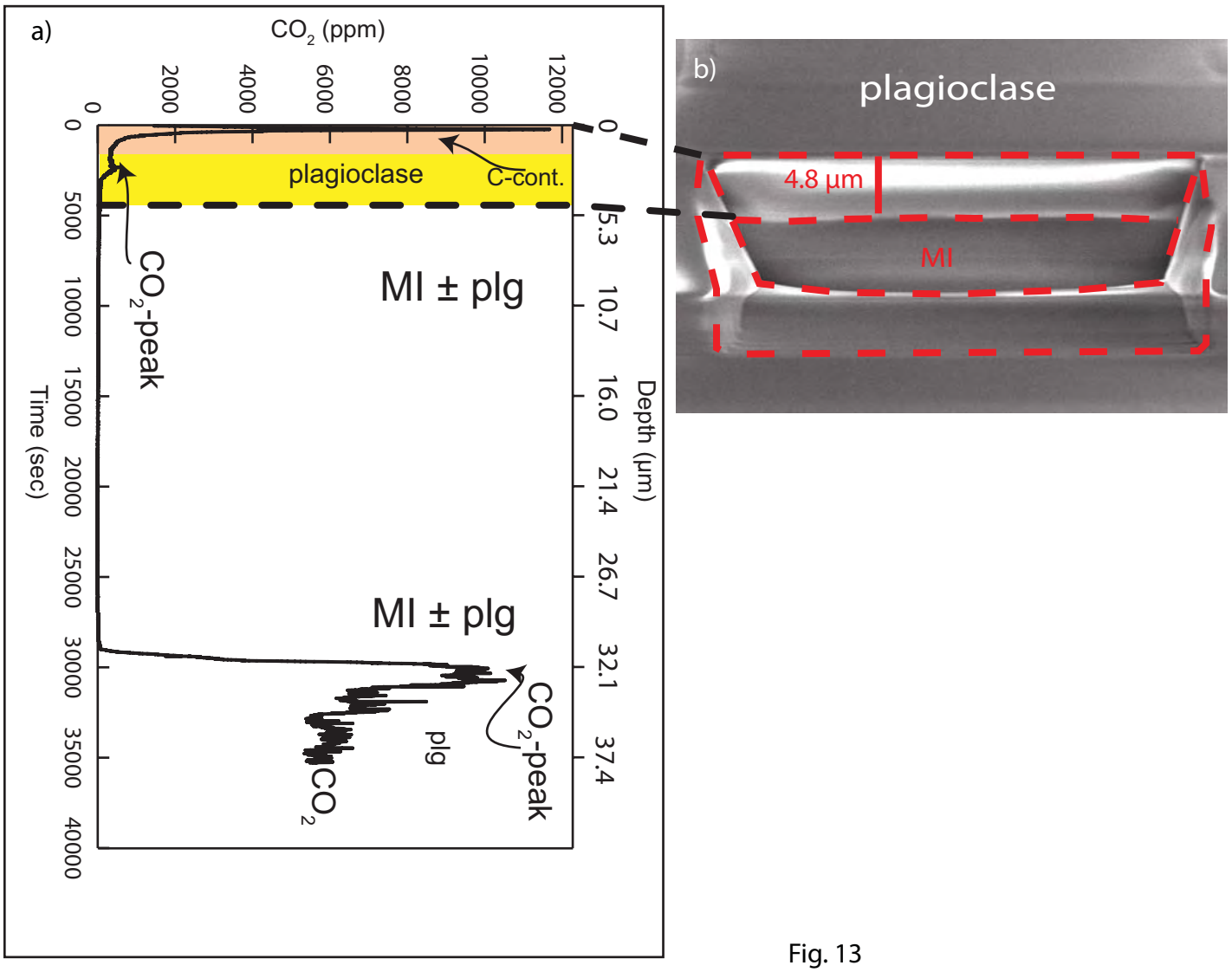


Fig. 13

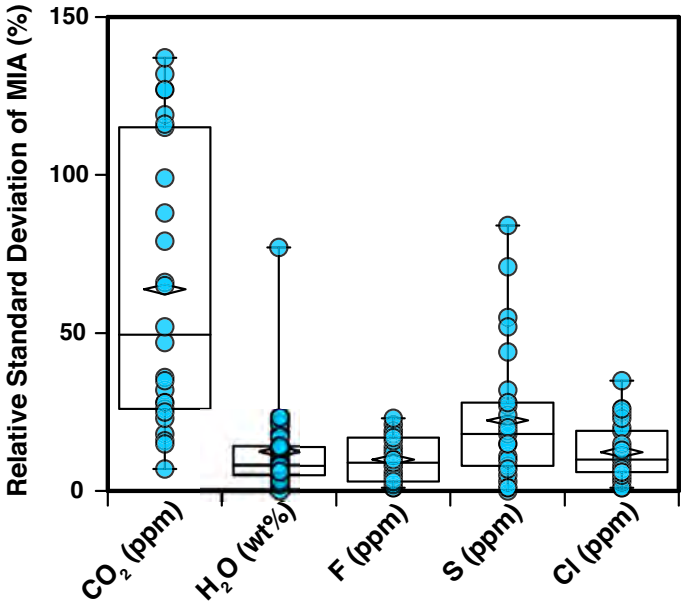
Relative Standard Deviation of MIA (%)
150
100
50
0
$CO_2$ (ppm)
$H_2O$ (wt%)
F (ppm)
S (ppm)
Cl (ppm)

Fig. 14

Table1. Corrected MI major-trace elements and volatiles concentrations of bubble-free MI of the same MIA hosted in olivine from Sol

| MI_ID | RESC5-O21-MA | RESC5-O21-ME |
|---|---|---|
| $SiO_2$ | 50.59 | 50.89 |
| $TiO_2$ | 1.42 | 1.39 |
| $Al_2O_3$ | 16.85 | 16.63 |
| $Fe_2O_3$ | 1.11 | 1.11 |
| FeO | 7.01 | 7.02 |
| MnO | 0.11 | 0.07 |
| MgO | 6.23 | 6.25 |
| CaO | 11.46 | 11.43 |
| $Na_2O$ | 2.60 | 2.63 |
| $K_2O$ | 2.17 | 2.12 |
| $P_2O_5$ | 0.44 | 0.47 |
| $Cr_2O_3$ | 0.03 | 0.00 |
| Be | bdl | bdl |
| B | bdl | bdl |
| V | 201.44 | 166.16 |
| Rb | 66.47 | 69.31 |
| Sr | 574.99 | 454.56 |
| Y | 25.27 | 20.05 |
| Zr | 117.09 | 99.76 |
| Nb | 18.15 | 13.77 |
| Cs | bdl | 2.88 |
| Ba | 684.98 | 542.33 |
| La | 17.84 | 16.79 |
| Ce | 47.32 | 33.08 |
| Pr | 6.56 | 4.04 |
| Nd | 33.33 | 19.24 |
| Sm | 12.37 | 4.26 |

| | | |
|---|---|---|
| Eu | 1.31 | 1.72 |
| Gd | 8.53 | 6.59 |
| Tb | 1.09 | 0.68 |
| Dy | 4.60 | 4.08 |
| Yb | 2.01 | 1.87 |
| Lu | bdl | 0.58 |
| Hf | bdl | 1.85 |
| Ta | 0.41 | 0.76 |
| Pb | 9.39 | 8.47 |
| Th | 4.20 | 4.01 |
| U | 1.84 | 0.96 |
| $CO_2$ | 1121 | 869 |
| $H_2O$ | 1.26 | 1.26 |
| F | 1318 | 1208 |
| S | 1272 | 1276 |
| Cl | 1803 | 1778 |
| $X_{ol}$ % | 6 | 6 |

bdl= below detection limit

$X_{ol}$ %= PEC (see Esposito et al., 2011 for calculation)

chiaro (data from Esposito et al., 2011)

Table 2. Representative analyses of volatile concentrations of MI from White Island and Solchiaro samples.

| MI ID | MIA ID | $CO_2$ (ppm) | $H_2O$ (wt%) | F (ppm) | S (ppm) | Cl (ppm) | host | woking session |
|---|---|---|---|---|---|---|---|---|
| REWI_15_A | MIA-10 | 172 | 0.4 | 401 | 60 | 903 | cpx | March_2010 |
| REWI_15_D | MIA-10 | 126 | 0.38 | 382 | 50 | 876 | cpx | March_2010 |
| REWI_15_H | MIA-10 | 106 | 0.4 | 415 | 131 | 975 | cpx | March_2010 |
| REWI_15_I | MIA-10 | 179 | 0.38 | 384 | 375 | 964 | cpx | March_2010 |
| WI_36_A | MIA-23 | 98 | 0.33 | 333 | 71 | 1380 | opx | December_2010 |
| WI_36_B | MIA-23 | 122 | 0.24 | 220 | 50 | 1339 | opx | December_2010 |
| WI_36_D | MIA-23 | 69 | 0.3 | 303 | 65 | 1266 | opx | December_2010 |
| WI_36_E | MIA-23 | 89 | 0.31 | 314 | 69 | 1302 | opx | December_2010 |
| RE-WI-29-A | MIA-27 | 46 | 0.45 | 305 | 45 | 897 | plg | February_2011 |
| RE-WI-29-C | MIA-27 | 52 | 0.46 | 340 | 58 | 1004 | plg | February_2011 |
| RE-WI-29-D | MIA-27 | 271 | 0.46 | 314 | 55 | 936 | plg | February_2011 |
| RE-WI-29-E | MIA-27 | 89 | 0.13 | 238 | 41 | 673 | plg | February_2011 |
| RE-WI-29-F | MIA-27 | 129 | 0.46 | 321 | 60 | 954 | plg | February_2011 |
| WI_25_A | MIA-19 | 87 | 0.33 | 254 | 45 | 1010 | plg | December_2010 |
| WI_25_C | MIA-19 | 192 | 0.3 | 229 | 33 | 748 | plg | December_2010 |
| WI_25_D | MIA-19 | 271 | 0.33 | 248 | 39 | 840 | plg | December_2010 |
| WI_25_F | MIA-19 | na | 0.34 | 261 | 44 | 837 | plg | December_2010 |
| WI_25_G | MIA-19 | 484 | 0.28 | 218 | 38 | 682 | plg | December_2010 |
| WI_25_I | MIA-19 | 270 | 0.3 | 229 | 41 | 769 | plg | December_2010 |
| WI_25_B | MIA-19 | 61 | 0.35 | 265 | 44 | 1019 | plg | December_2010 |
| WI_25_E* | MIA-19 | 1418 | 0.34 | 251 | 41 | 827 | plg | December_2010 |
| RESC5_O27_F1 | MIA-35 | 447 | 1.80 | 1471 | 1600 | 2732 | olivine | VT_Oct_2011 |
| RESC5_O27_F2 | MIA-35 | 448 | 1.82 | 1472 | 1621 | 2794 | olivine | VT_Oct_2011 |
| RESC5_O27_C | MIA-35 | 361 | 1.45 | 1000 | 1305 | 2572 | olivine | VT_Oct_2011 |
| RESC5-O27-MG | MIA-35 | 673 | 1.31 | 1210 | 1266 | 1824 | olivine | WHOI Feb_2011 |
| RESC5-O27-MF | MIA-35 | 718 | 0.99 | 940 | 995 | 1229 | olivine | WHOI Feb_2011 |
| RESC5-O27-MF | MIA-35 | 552 | 1.24 | 1259 | 1571 | 2818 | olivine | VT Dec_2010 |

| | | | | | | | | |
|---|---|---|---|---|---|---|---|---|
| RESC5-O27_F1 | MIA-35 | 507 | 1.24 | 1238 | 1563 | 2796 | olivine | VT Dec_2010 |
| RESC5-O27_G | MIA-35 | 490 | 1.20 | 1285 | 1532 | 2734 | olivine | VT Dec_2010 |
| RESC5-O27_E | MIA-35 | 450 | 1.23 | 1286 | 1134 | 2916 | olivine | VT Dec_2010 |
| RESC5_O27_F | MIA-35 | 509 | 1.19 | 1365 | 1418 | 2042 | olivine | VT Mar_2010 |
| RESC5_O27_F1 | MIA-35 | 493 | 1.17 | 1350 | 1411 | 2019 | olivine | VT Mar_2010 |
| RESC5_O27_G | MIA-35 | 645 | 1.08 | 1266 | 1299 | 1892 | olivine | VT Mar_2010 |
| RESC5-O27_B[#] | MIA-35 | 358 | 1.27 | 1026 | 1384 | 2730 | olivine | VT Jul_2009 |

*MI measured more than one time; na = not available; cpx = clinopyroxene; opx = orthopyroxene; plg = plagioclase: oli = olivine.
[#]data by Esposito et al. (2011)

| type of MI | shape of MI | type of MIA |
|---|---|---|
| 1 | ovoid | azonal/core |
| 1 | ovoid | azonal/core |
| 1 | ovoid | azonal/core |
| 4 | ovoid | azonal/core |
| 1 | ovoid | zonal |
| 1 | ovoid | zonal |
| 1 | ovoid | zonal |
| 1 | ovoid | zonal |
| 2 | Irregular | azonal/core |
| 2 | Irregular | azonal/core |
| 1 | Irregular | azonal/core |
| 1 | negative crystal shape | azonal/core |
| 1 | negative crystal shape | azonal/core |
| 1 | negative crystal shape | azonal/core |
| 1 | negative crystal shape | azonal/core |
| 1 | negative crystal shape | azonal/core |
| 1 | negative crystal shape | azonal/core |
| 1 | negative crystal shape | azonal/core |
| 1 | negative crystal shape | azonal/core |
| 1 | negative crystal shape | azonal/core |
| 1 | negative crystal shape | azonal/core |
| 1 | irregular | azonal/core |
| 1 | irregular | azonal/core |
| 1 | ovoid | azonal/core |
| 1 | ovoid | azonal/core |
| 1 | irregular | azonal/core |
| 1 | irregular | azonal/core |

| | | |
|---|---|---|
| 1 | irregular | azonal/core |
| 1 | ovoid | azonal/core |
| 1 | irregular | azonal/core |
| 1 | irregular | azonal/core |
| 1 | irregular | azonal/core |
| 1 | ovoid | azonal/core |
| 1 | ovoid | azonal/core |

| | $CO_2$ (ppm) | $H_2O$ (wt%) | F (ppm) | S (ppm) | Cl (ppm) | host |
|---|---|---|---|---|---|---|
| RSD-MIA-37 | 18% | 0% | 6% | 0% | 1% | olivine |
| RSD-MIA-35 | 32% | 10% | 13% | 3% | 12% | olivine |
| RSD-MIA-33 | 7% | 3% | 3% | 28% | 3% | orthopyroxene |
| RSD-MIA-32 | 28% | 9% | 8% | 10% | 10% | plagioclase |
| RSD-MIA-30 | na | 23% | 19% | 19% | 11% | clinopyroxene |
| RSD-MIA-28 | 115% | 5% | 3% | 7% | 10% | plagioclase |
| RSD-MIA-27 | 26% | 77% | 21% | 27% | 24% | plagioclase |
| RSD-MIA-26 | 66% | 7% | 1% | 5% | 5% | clinopyroxene |
| RSD-MIA-25 | 127% | 3% | 3% | 11% | 7% | orthopyroxene |
| RSD-MIA-24 | na | 7% | 1% | 8% | 4% | plagioclase |
| RSD-MIA-23 | 23% | 13% | 17% | 15% | 4% | orthopyroxene |
| RSD-MIA-22 | na | 2% | 1% | 1% | 1% | plagioclase |
| RSD-MIA-20 | 36% | 4% | 2% | 21% | 8% | orthopyroxene |
| RSD-MIA-19 | 119% | 8% | 7% | 10% | 14% | plagioclase |
| RSD-MIA-18 | 88% | 12% | 12% | 15% | 19% | plagioclase |
| RSD-MIA-17 | 132% | 18% | 18% | 24% | 26% | plagioclase |
| RSD-MIA-16 | 116% | 21% | 8% | 32% | 20% | clinopyroxene |
| RSD-MIA-14 | 137% | 21% | 19% | 18% | 13% | plagioclase |
| RSD-MIA-13 | 127% | 6% | 5% | 7% | 5% | plagioclase |
| RSD-MIA-12 | 28% | 7% | 10% | 84% | 25% | clinopyroxene |
| RSD-MIA-10 | 25% | 3% | 4% | 55% | 6% | clinopyroxene |
| RSD-MIA-09 | 47% | 14% | 16% | 19% | 15% | plagioclase |
| RSD-MIA-08 | 79% | 17% | 18% | 20% | 23% | plagioclase |
| RSD-MIA-05 | 99% | 13% | 17% | 52% | 26% | clinopyroxene |
| RSD-MIA-04 | 65% | 23% | 23% | 71% | 35% | clinopyroxene |
| RSD-MIA-03 | 16% | 8% | 9% | 28% | 6% | orthopyroxene |
| RSD-MIA-02 | 15% | 6% | 3% | 1% | 6% | clinopyroxene |
| RSD-MIA-01 | 52% | 14% | 10% | 15% | 13% | clinopyroxene |

| | | | | | |
|---|---|---|---|---|---|
| RSD max | 137% | 77% | 23% | 84% | 35% |
| RSD min | 7% | 0% | 1% | 0% | 1% |
| RSD average | 65% | 13% | 10% | 22% | 13% |
| RSD median | 52% | 8% | 8% | 16% | 10% |

Table 3. Volatile compositions of MI from the Solchiaro volcano measured multiple times during different working sessions.

| MI-ID | $CO_2$ | $H_2O$ | F | S | Cl |
|---|---|---|---|---|---|
| RESC5-O27-MF-WHOI-Feb-2011 | 718 | 0.99 | 940 | 995 | 1229 |
| RESC5-O27-MF-VT-Dec-2010 | 529 | 1.24 | 1248 | 1567 | 2807 |
| RESC5-O27-MF-VT-Mar-2010 | 501 | 1.18 | 1358 | 1415 | 2031 |
| RESC5-O27-MF-VT-Oct-2011 | 447 | 1.81 | 1471 | 1610 | 2763 |
| average | 549 | 1.30 | 1254 | 1397 | 2208 |
| stdev | 118 | 0.35 | 228 | 280 | 743 |
| relative stdev | 21% | 27% | 18% | 20% | 34% |
| | | | | | |
| RESC5-O27-MG-WHOI-Feb-2011 | 673 | 1.31 | 1210 | 1266 | 1824 |
| RESC5-O27-MG-VT-Dec-2010 | 490 | 1.2 | 1285 | 1532 | 2734 |
| RESC5-O27-MG-VT-Mar-2010 | 645 | 1.08 | 1266 | 1299 | 1892 |
| average | 603 | 1.20 | 1254 | 1366 | 2150 |
| stdev | 99 | 0.12 | 39 | 145 | 507 |
| relative stdev | 16% | 10% | 3% | 11% | 24% |

Table 4. Volatile compositions of MI from White Island of sample (1986 and 1988 eruptions) prepared and measured at the Woods Hole Oc

| sample id | $CO_2$ (ppm) | $H_2O$ (wt%) | F (ppm) | S (ppm) | Cl (ppm) |
|---|---|---|---|---|---|
| MI from 1986-eruption | | | | | |
| MI-1 | 31 | 0.61 | 402 | 47 | 855 |
| MI-3 | 19 | 0.49 | 427 | 50 | 959 |
| MI-5 | 160 | 0.55 | 431 | 56 | 1005 |
| MI-6 | 91 | 0.38 | 406 | 55 | 987 |
| MI-7 | 21 | 0.53 | 381 | 45 | 907 |
| MI-8 | 512 | 0.59 | 413 | 61 | 769 |
| MI-8-2 | 312 | 0.61 | 424 | 62 | 798 |
| MI-9 | 49 | 0.53 | 406 | 66 | 982 |
| MI-11 | 197 | 0.53 | 484 | 260 | 1205 |
| MI-12 | 50 | 0.52 | 402 | 295 | 970 |
| MI-13 | 145 | 0.54 | 417 | 68 | 918 |
| MI-17 | 46 | 0.60 | 501 | 185 | 936 |
| MI-18 | 81 | 0.55 | 459 | 316 | 930 |
| | | | | | |
| MI from 1988-eruption | | | | | |
| 880-2 | 194 | 0.59 | 378 | 288 | 1246 |
| 880-3 | 51 | 0.62 | 392 | 83 | 947 |
| 880-4 | 22 | 0.56 | 438 | 52 | 827 |
| 880-5 | 32 | 0.53 | 409 | 129 | 924 |
| 880-6 | 58 | 0.54 | 337 | 55 | 976 |
| 880-7 | 107 | 0.69 | 533 | 103 | 740 |
| 880-8 | 13 | 0.54 | 388 | 677 | 1010 |
| 880-10 | 91 | 0.60 | 392 | 79 | 953 |
| 880-11 | 47 | 0.61 | 402 | 67 | 982 |
| 880-12 | 15 | 0.48 | 352 | 55 | 1010 |
| 880-13 | 207 | 0.63 | 522 | 331 | 804 |

| | | | | | |
|---|---|---|---|---|---|
| 880-14 | 60 | 0.57 | 364 | 141 | 941 |
| 880-15 | 32 | 0.52 | 378 | 54 | 936 |
| 880-16 | 35 | 0.57 | 406 | 105 | 970 |
| 880-20 | 62 | 0.51 | 409 | 316 | 1114 |
| 880-21 | 29 | 0.61 | 399 | 302 | 1114 |
| 880-22 | 263 | 0.61 | 374 | 220 | 947 |

eanographic Institution SIMS laboratory. In green is the MI (860210-MI-8 and MI8-2) showing the highest $CO_2$ concentration decreasing wi

This is a preprint, the final version is subject to change, of the American Mineralogist (MSA)
Cite as Authors (Year) Title. American Mineralogist, in press.
(DOI will not work until issue is live.) DOI: http://dx.doi.org/10.2138/am.2014.4574

th depth (from 608 to 282 ppm, see Deposit Item-04).